Li *et al.*
Chinese Journal of Mechanical Engineering (2024) 37:18
https://doi.org/10.1186/s10033-024-01005-9

Chinese Journal of Mechanical Engineering

ORIGINAL ARTICLE

Open Access

Effect of Interface Form on Creep Failure and Life of Dissimilar Metal Welds Involving Nickel-Based Weld Metal and Ferritic Base Metal

Xiaogang Li[1*], Junfeng Nie[1*], Xin Wang[1], Kejian Li[2] and Haiquan Zhang[1]

Abstract

For dissimilar metal welds (DMWs) involving nickel-based weld metal (WM) and ferritic heat resistant steel base metal (BM) in power plants, there must be an interface between WM and BM, and this interface suffers mechanical and microstructure mismatches and is often the rupture location of premature failure. In this study, a new form of WM/BM interface form, namely double Y-type interface was designed for the DMWs. Creep behaviors and life of DMWs containing double Y-type interface and conventional I-type interface were compared by finite element analysis and creep tests, and creep failure mechanisms were investigated by stress-strain analysis and microstructure characterization. By applying double Y-type interface instead of conventional I-type interface, failure location of DMW could be shifted from the WM/ferritic heat-affected zone (HAZ) interface into the ferritic HAZ or even the ferritic BM, and the failure mode change improved the creep life of DMW. The interface premature failure of I-type interface DMW was related to the coupling effect of microstructure degradation, stress and strain concentrations, and oxide notch on the WM/HAZ interface. The creep failure of double Y-type interface DMW was the result of Type IV fracture due to the creep voids and micro-cracks on fine-grain boundaries in HAZ, which was a result of the matrix softening of HAZ and lack of precipitate pinning at fine-grain boundaries. The double Y-type interface form separated the stress and strain concentrations in DMW from the WM/HAZ interface, preventing the trigger effect of oxide notch on interface failure and inhibiting the interfacial microstructure cracking. It is a novel scheme to prolong creep life and enhance reliability of DMW, by means of optimizing the interface form, decoupling the damage factors from WM/HAZ interface, and then changing the failure mechanism and shifting the failure location.

Keywords Dissimilar metal weld, Nickel-based weld metal, Ferritic heat resistant steel, Interface, Creep strain, Microstructure, Failure mechanism, Creep life

1 Introduction

Ferritic heat resistant steels with good performance and low cost have been widely used to fabricate key components in power plans [1–5]. Among them, martensitic steel containing ~ 9%Cr and low alloy bainitic steel containing ~ 2%Cr are the main materials selected [6–8]. For flexible material selection and cost savings, martensitic steel or bainitic steel is always joined with nickel-based alloy or austenitic stainless steel by means of welding, and thus there are thousands of dissimilar metal welds (DMWs) in coal-fired power plants and nuclear power plants [6, 7, 9–12]. Nickel-based alloy or austenitic

*Correspondence:
Xiaogang Li
xiaogangli@mail.tsinghua.edu.cn
Junfeng Nie
niejf@tsinghua.edu.cn
[1] Institute of Nuclear and New Energy Technology, Key Laboratory of Advanced Reactor Engineering and Safety of Ministry of Education, Tsinghua University, Beijing 100084, China
[2] Department of Mechanical Engineering, Tsinghua University, Beijing 100084, China

stainless steel with better resistance of creep and oxidation is employed in high temperature position of the unit, and martensitic steel or bainitic steel is employed in low temperature position to save costs [13–15]. Initially, the filler metal made of austenitic stainless steel was selected to manufacture the DMWs [16]. At the interface between austenitic weld metal (WM) and ferritic steel base metal (BM), there would be stress concentration and serious carbon migration during long term high temperature exposure, which were caused by large difference of coefficient of thermal expansion (CTE) on both sides of the interface and huge chemical potential gradient respectively [7]. It should be noted that ferritic steel side in the DMW was weak due to its relatively poor mechanical properties, in which BM, heat-affected zone (HAZ), and the interface between HAZ and WM were three possible failure locations [17]. When the failure locaiton was in the ferritic BM, the fracture behavior of DMW was controlled by plastic deformation and was a result of growth and coalescence of dimples. However, when the failure occurred in the ferritic HAZ or along the WM/ferritic HAZ interface, the creep strength and life of the DMW was be much lower than that of the ferritic BM, and there was no obvious plastic deformation before the failure, which was difficult to predict the failure time [17]. Type IV crack led to the ferritic HAZ failure of DMW [18], which was related with matrix softening, precipitate coarsening and lack of precipitate pinning at grain boundaries [18–23]. Type IV crack in HAZ could be effectively suppressed by adding B element to the steel or adopting suitable post-weld heat treatment (PWHT) [8, 24, 25]. However, there is still no effective way to avoid WM/HAZ interface failure. Meanwhile, the creep life of DMW failed along the WM/HAZ interface was further lower than that failed in HAZ under same creep condition [17].

In the process of engineering application and scientific research, it was found that premature failure of the above DMWs always occurs along the WM/ferritic HAZ interface [7, 9, 26, 27]. The interface premature failure in DMWs would lead to forced plant outages, which costs a power company up to $850000/day in lost revenue [28]. Failure has always been a focus of concern in the field of weld [29–33]. Recently, the filler metal made of nickel-based alloy has been widely used to manufacture the DMWs. The service life and performance of the DMW with nickel-based WM are obviously better than that of the DMW with austenitic WM [16, 34, 35], which is due to reducing the interface stress and carbon migration. However, the interface premature failure in DMWs still existed after the nickel-based filler metal was adopted, because the difference of CTE between WM and BM and the chemical potential gradient near the WM/BM interface still existed. Thus, avoiding interface failure and extending life of DMWs will always be a concern for the reliability of power plants.

Understanding the failure mechanism is the prerequisite of putting forward a reasonable scheme of prolonging life of DMW. Earlier researches suggested that the interface failure in the DMW was related to interfacial stress concentration [7, 36, 37], oxide notch [7, 26, 38], microstructure degradation [39, 40], creep voids around interfacial carbides [7, 41, 42] and creep strength gradient [12]. In summary, interface failure is the result of the coupling effect of three factors, namely interfacial stress, interfacial microstructure and high temperature oxidation. Interfacial stress and microstructure was determined by the different chemical compositions and properties of the dissimilar materials. High temperature oxidation was inevitable for the DMWs used in power plants. Thus, it is not realistic to prolong the DMW life by completely avoiding any of above three factors. Zhang et al. [43] compared creep behaviors of the DMW fabricated by Inconel 617 filler metal and the DMW fabricated by Inconel 82 filler metal, and they found that the latter had a longer creep life, which was due to its lower creep strength gradient across the WM/ferritic HAZ interface. Hu et al. [44] investigated the effects of weld angle on the creep life of DMW by finite element analysis (FEA), and they noted that the DMW had longer life after adopting weld angles smaller than 45° than that of standard 90° welded components, however, the influences of microstructure and oxidation were not considered during the study. Wang et al. [45] added a CrN coating by the physical vapor deposition technique at the nickel-based WM/matensitic steel interface to inhibit the occurrence of surface cracks, but many cracks were still formed on subsurface. Recently, graded transition joint (GTJ) were developed to obtain the interface with absence steep chemical composition gradient, and it was expected to avoid interface failure and to prolong creep life [46]. In the process of preparing GTJ, ferritic HAZ repeatedly suffered welding thermal cycle, and the carbides in the HAZ were thus coarsened [47]. In addition, the Ni-rich martensite was still inevitably formed near the WM/ferritic HAZ interface [48], which was conducive to the occurrence of interface failure. Thus, the GTJ was not an effective scheme for creep life extension [47, 48]. The feasible solution for life extension of DMW is limitedly reported. Therefore, it is urgent to propose a reasonable life extension scheme based on failure mechanism analysis and it is necessary to demonstrate and verify the validity of the scheme.

In this study, we innovatively proposed a scheme for prolonging the DMW creep life by optimizing the interface form, and a new nickel-based WM/ferritic HAZ

interface form for DMW, namely double Y-type interface, was designed. Firstly, FEA method was used to investigate the stress and strain in novel double Y-type interface joint and conventional I-type interface joint, and we quantitatively compared the evolution of mechanical states and the creep life of DMW during long term high temperature exposure. Furthermore, the DMWs with the above two kinds of interfaces were fabricated by welding, and the creep tests were carried out respectively. After creep tests, the broken samples were analyzed by optical microscopy (OM), scanning electron microscopy (SEM), electron backscatter diffraction (EBSD) and energy dispersive X-ray (EDX) to clarify the effects of microstructure and oxidation on failure. Meanwhile, the hardness profile in the DMWs before and after creep was characterized to analyze its effect on creep behavior. Finally, the effects of interface form on creep failure and life of the DMWs were discussed by considering the mechanical state, microstructure and oxidation.

2 Materials and Methods

The main material used in this study was martensitic heat resistant steel containing ~ 9%Cr (hereinafter referred to 9Cr steel), which was as ferritic BM for DMW fabrication. The chemical composition (wt. %) of 9Cr steel is 9.85 Cr, 0.11 C, 0.45 Mn, 1.04 Mo, 1.00 W, 0.18 V, 0.06 Si, 0.73 Ni, 0.05 Nb, 0.004 Al, 0.05 N and Fe balanced. The BM on the other side of the DMW was nickel-based alloy. The chemical composition (wt. %) of nickel-based alloy is 22.38 Cr, 0.05 C, 9.02 Mo, 12.05 Co, 0.01 Mn, 0.03 Nb, 0.04 Si, 1.02 Al, 0.004 N, 0.005 Cu, 0.44 Ti, 0.33 Fe and Ni balance. Tungsten inert gas (TIG) welding was used for manufacturing the DMW between 9Cr steel and nickel-based alloy. Filler metal was Inconel 82 nickel-based wire. The chemical composition (wt. %) of Inconel 82 is 20 Cr, 0.01 C, 3.0 Fe, 3.2 Mn, 2.48 Nb, 0.37 Ti, 0.01 Cu, 0.03 Co, 0.05 Si and Ni balance. The arc voltage, welding current and welding speed were 12 V, 200 A and 90 mm/min respectively. After welding, the DMWs were subjected to PWHT at 690 ℃ for 10 h to relieve residual stress.

The DMW including I-type interface between WM and 9Cr BM and the DMW including double Y-type interface between WM and 9Cr BM were subjected for creep test at 600 ℃/140 MPa, until they were completely broken. The axis of cylindrical creep sample was perpendicular to the welding direction, which contained WM, HAZ and BMs. The length of cylindrical creep sample was 120 mm and the diameter of gauge section was 8 mm. After creep tests, the microstructure and chemical composition on the failure path were analyzed by OM, SEM and EDX. The fracture appearance of the broken sample was observed by SEM. The sample for failure path observation was grinded to 5000 grit, mechanically polished to a 2.5 μm surface and chemically etched. The solution used for etching was Villela's reagent (100 mL ethanol + 5 mL HCl + 1 g picric acid), and only the ferritic steel side in the DMW was chemically etched. To further investigate creep damage and creep strain, EBSD was performed for the crept sample. The sample for EBSD observation was mechanically polished and ion beam polished. Ion beam polishing was carried out using an ion beam milling system at 2–6 kV voltages and 1.3–2.5 mA gun currents. In addition, hardness tests were carried out in the DMWs before and after creep test by means of a Vickers hardness tester (FM 800) with a load of 200 g and a holding time of 10 s.

In order to obtain the evolution of stress and strain in the DMWs during creep and to preliminarily analyze whether changing the interface form was conducive to improving the DMW life, FEA method was used to simulate the creep process of different DMWs containing I-type interface and double Y-type interface. Axisymmetric FEA model in accordance with the creep sample dimension was built using Abaqus 2020 software. The FEA model contained WM, HAZ and BM, and the axis of it was perpendicular to the welding direction. The HAZ was simplified into coarse-grained heat-affected zone (CGHAZ) and inter-critical heat-affected zone (ICHAZ), and it is assumed that the transition of properties of BM, WM and different HAZ zones was abrupt. The model was built by setting WM part with material parameters of Inconel 82 and BM part with material parameters of 9Cr steel. The FEA process contained three steps: (1) Loading temperature from room temperature to 600 ℃; (2) Increasing creep load from 0 MPa to 80 MPa; (3) Creep process (up to sample failure). In the process of load holding, one end of the sample was fixed and the other end was subjected to uniform tensile stress.

3 Results and Discussion

The DMW containing 9Cr steel cannot be immune to the Type crack in HAZ and the interfacial crack, which determines that the DMW life was closely related to the crack mode. It could be inferred that there would be the competition of creep damage in the HAZ and near the interface. The pervious literatures indicated that the failure mode and creep life of DMW were related to service temperature and stress level [17, 27, 41], and in this study we noted that the effects of WM/HAZ interface form on creep failure and life of DMW. Especially, the correlation between interface form and failure mechanism was clarified.

3.1 Effect of Interface Form on Creep Life and Failure by Means of FEA Models and Simulation

In this section, the creep sample of welded joint containing I-type interface and the creep sample of welded joint containing double Y-type interface were modeled in ABAQUS, and FEA on the creep damage and failure process was conducted. The influences of different interface forms on the creep life were analyzed, which provided theoretical support for further creep experiment verification.

Two kinds of interface forms were designed for comparative study: (1) The interface between WM and 9Cr steel was perpendicular to the external load direction, namely I-type interface; (2) Form of the interface between WM and 9Cr steel was similar to double Y, namely double Y-type interface. The design purpose of interface form (1) was to make the interface perpendicular to the loading and the it was most prone to type I fracture [49], which was the most dangerous form of failure in practical engineering. The double Y-type interface was a novel interface form, which could be practically realized by cap welding along the interface between WM and 9Cr steel.

3.1.1 FEA Models of the Creep Sample Containing I-type Interface and the Creep Sample Containing Double Y-type Interface

As shown in Figure 1, the FEA models containing I-type interface (see Figure 1(a)) and double Y-type interface (see Figure 1(b)) were built in accordance with the sample shape and dimension for subsequent creep tests, and the similar ideal model was used by Zhang et al. [43]. The above FEA models were mainly used to analyze the effect of forms of interface between nickel-based WM and 9Cr steel on the creep life and failure, and thus the BMs on both sides were setting as 9Cr steel. The FEA models consisted of BM, CGHAZ, ICHAZ and WM. The width of CGHAZ and ICHAZ was set as 1.5 mm. The statistical data for stress and strain analyses were extracted along sample surface (path 1 in Figures 1(c) and 1(d)) and sample middle (path 2 in Figure 1(c) and (d)). The previous studies [17, 50] indicated that oxide notch formed at the interface would promote interface failure. After the oxide notch was formed, the oxide in the notch would fall off [17], and thus oxide notch was simplified as a notch in the FEA model. After the creep time of 1000 h, the specified elements at the WM/HAZ interface were removed

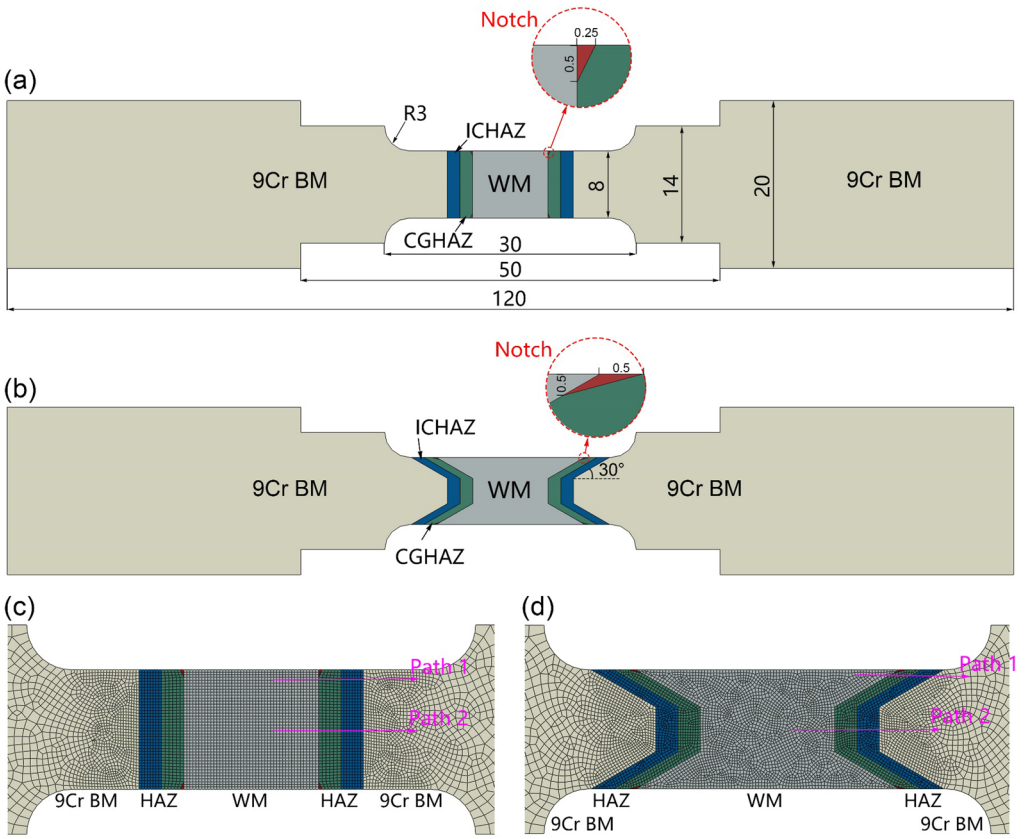

Figure 1 FEA models for creep samples containing different interface forms: (**a**) I-type interface sample, (**b**) Double Y-type interface sample, (**c**) Mesh of the I-type interface sample and paths for extracting data, (**d**) Mesh of the double Y-type interface sample and paths for extracting data

to form the interface notch. The creep load was set at 80 MPa and the temperature was set at 600 ℃. The material parameters were from the literatures [36, 51, 52]. The creep strain rate of CGHAZ was set as equal to 9Cr steel and the creep strain rate of ICHAZ was set as equal to an order of magnitude higher than 9Cr steel [53]. The subroutine was written in Fortran to realize the creep damage initialization and evolution in FEA.

3.1.2 Stress and Strain Analyses during Creep Processes

Figure 2 shows equivalent creep strain and Mises stress contours for the samples containing I-type interface and double Y-type interface after creep for 1000 h. At this time, the interface notch had not been considered. For the joint containing I-type interface, the creep strain at WM/HAZ interface was high near the sample surface, while that at WM/HAZ interface was low near the sample middle, as shown in Figure 2(a). Meanwile, Mises stress at WM/HAZ interface near the sample surface was also high, as marked by the black circles in Figure 2(b) with a maximum value of 281 MPa. For the joint containing double Y-type interface, the creep strain mainly concentrated in the ICHAZ, but not at the WM/HAZ interface, as shown in Figure 2(c). Meanwhile, the hightest Mises stress was 255 MPa in the whole double Y-type interface joint. Hence, the double Y-type interface joint could effectively redeuce the creep strain concentration and stress concentration at the WM/HAZ interface.

Figure 3 shows equivalent creep strain and Mises stress contours for the samples containing I-type

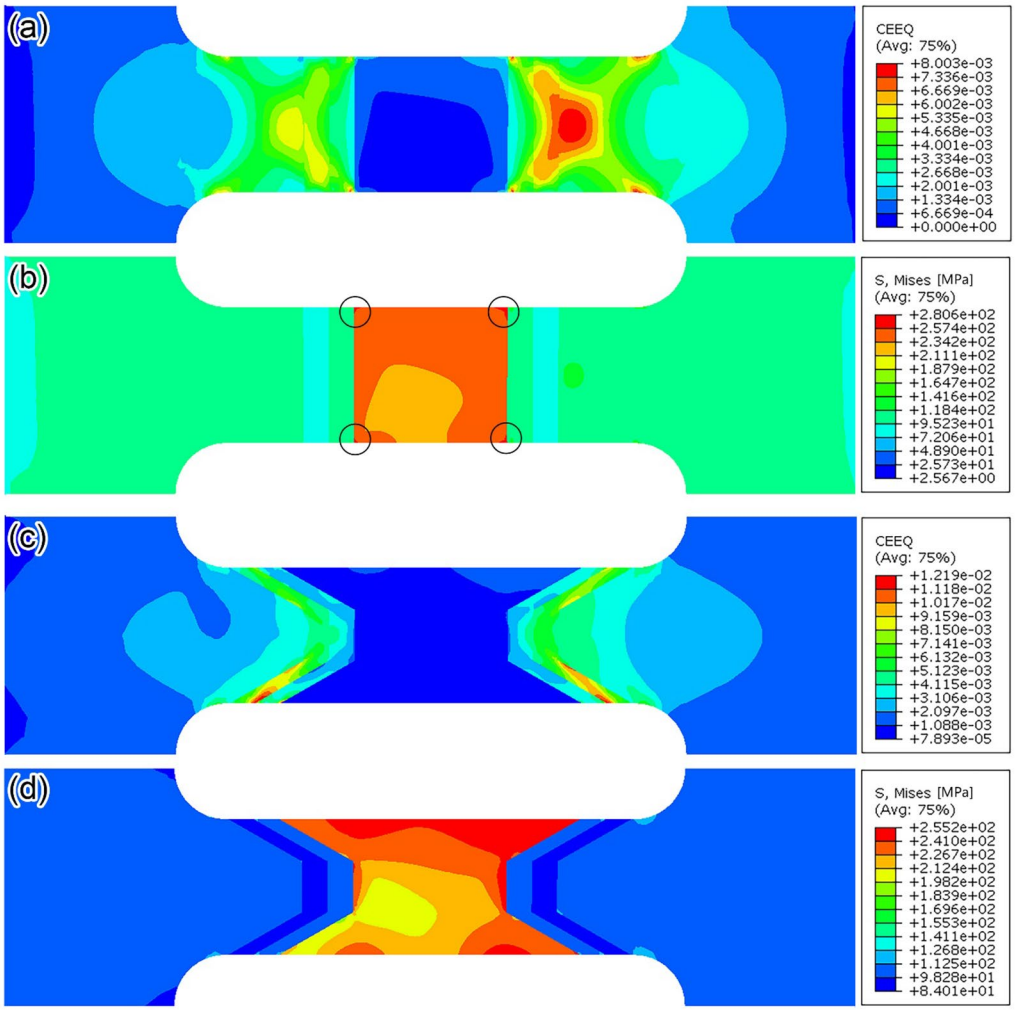

Figure 2 Equivalent creep strain and Mises stress distributions for samples containing different interface forms after creep for 1000 h at 600 ºC/80 MPa: (**a**) Equivalent creep strain contour for I-type interface sample, (**b**) Mises stress contour for I-type interface sample, (**c**) Equivalent creep strain contour for double Y-type interface sample, (**d**) Mises stress contour for double Y-type interface sample

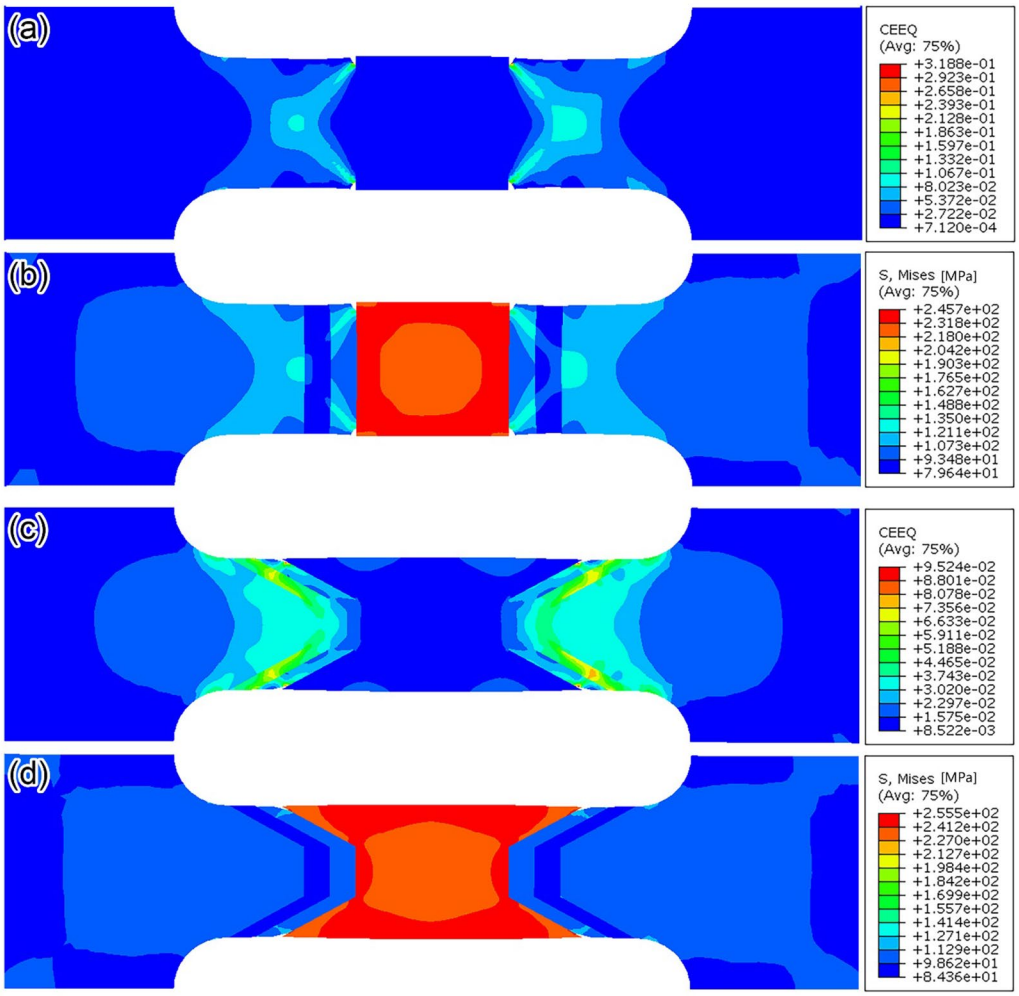

Figure 3 Equivalent creep strain and Mises stress distributions for samples containing different interface forms after creep for 10000 h at 600 ℃/80 MPa: (**a**) Equivalent creep strain contour for I-type interface sample, (**b**) Mises stress contour for I-type interface sample, (**c**) Equivalent creep strain contour for double Y-type interface sample, (**d**) Mises stress contour for double Y-type interface sample

interface and double Y-type interface after creep for 10000 h, at which time the interface notch had existed for 9000 h. For the joint containing I-type interface, obvious creep deformation occurred at the tip of interface notch, as shown in Figure 3(a). Meanwhile, stress concentration also existed at the interface notch tip, as shown in Figure 3(b). It could be inferred that stress concentration at the interface notch tip would accelerate the creep strain concentration at this position. For the joint containing double Y-type interface, creep strain mainly concentrated near ICHAZ/BM, as shown in Figure 3(c), and WM bore some deformation. Meanwhile, no obvious stress concentration occurred at the WM/HAZ interface and in the HAZ, as shown in Figure 3(d). It indicated that the WM/HAZ interface region of double Y-type interface joint was not subjected to stress and strain concentrations at the same time.

3.1.3 Creep Life of Samples Containing Different Interface Forms

The I-type interface sample completely broke and failed after 23087 h, and the double Y-type interface sample completely broke and failed after 40088 h. The creep life of double Y-type interface sample was 1.7 times that of I-type interface sample. Figure 4 shows creep strain and stress contours before final failure. Figure 4(a) and (b) show the equivalent creep strain and Mises stress distributions in the I-type interface sample. The creep strain concentration near WM/HAZ interface and in ICHAZ was serious in the I-type interface joint, and the failure mainly occurred in the above positions. Figure 4(c) and (d) show the

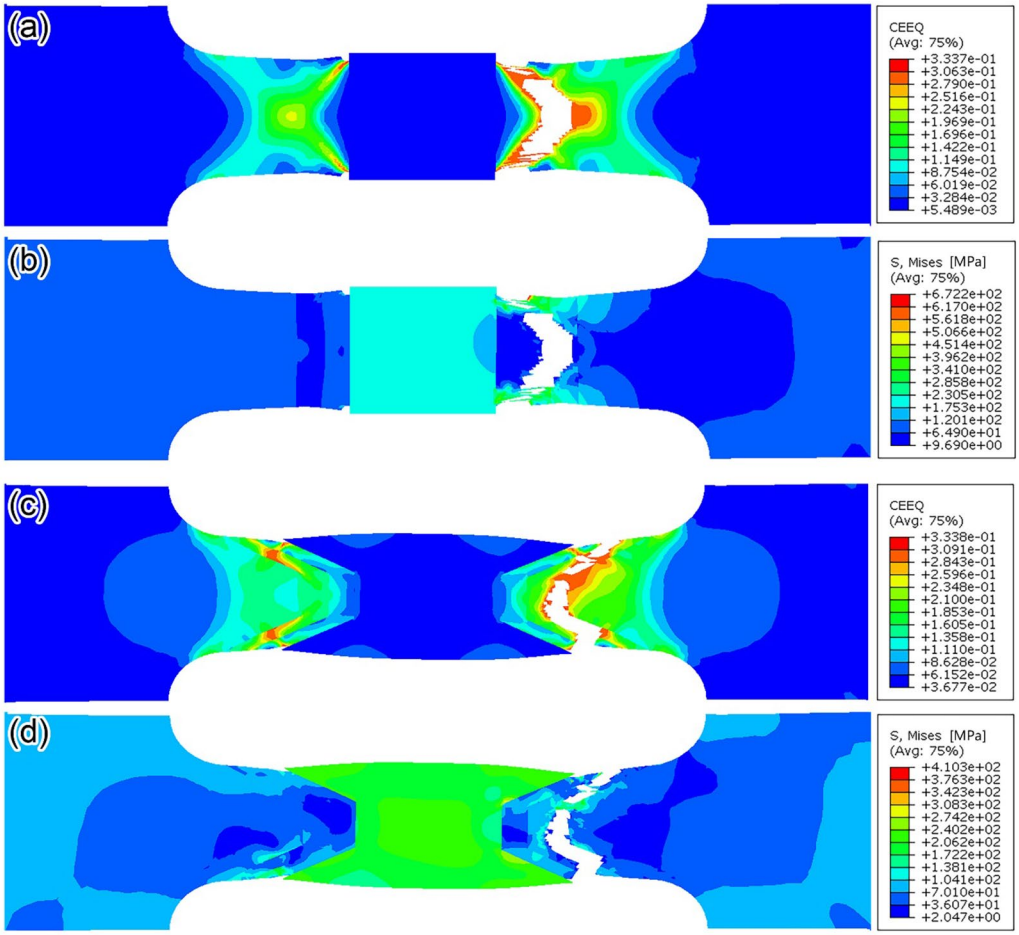

Figure 4 Equivalent creep strain and Mises stress distributions for samples before complete failure: (**a**) Equivalent creep strain contour for I-type interface sample after creep for 23085 h, (**b**) Mises stress contour for I-type interface sample after creep for 23085 h, (**c**) Equivalent creep strain contour for double Y-type interface sample after creep for 40086 h, (**d**) Mises stress strain contour for double Y-type interface sample after creep for 40086 h

equivalent creep strain and Mises stress distributions in the double Y-type interface sample. The creep strain in ICHAZ and its nearby BM was large in the double Y-type interface joint, and the failure mainly occurred at above positions. Crack in the sample middle propagated into the BM, as shown in Figure 4(c). More specially, the nickel-based WM had plastic deformation, as shown in Figure 4(c). The stress concentration was not obvious at the WM/HAZ interface in double Y-type interface joint, as shown in Figure 4(d).

Compared with the I-type interface, the double Y-type interface could lead the creep failure position of the joint from the WM/HAZ interface to the HAZ or even the BM, and it prolonged the creep life. Meanwhile, the double Y-type interface could suppress the promoting effect of interface notch on interface failure. In addition, the double Y-type interface joint exhibited large plastic deformation before failure.

3.1.4 Quantitative Analysis of Evolutions of Stress and Strain Near the WM/HAZ Interface during Creep

In order to quantitatively analyze the mechanical state evolutions in joints with different interface forms during creep process, equivalent creep strain and Mises stress data were extracted along paths of sample surface (path 1 in Figure 1(c) and (d)) and sample middle (path 2 in Figure 1(c) and (d)), and the results are shown in Figures 5 and 6.

Figure 5(a) shows the change in equivalent creep strain near sample surface from 5000 h to 20000 h in the I-type interface joint. The creep strain mainly concentrated at the WM/HAZ interface, and the interface creep strain concentration became more and more serious with the extension of creep time, as shown in Figure 5(a). The

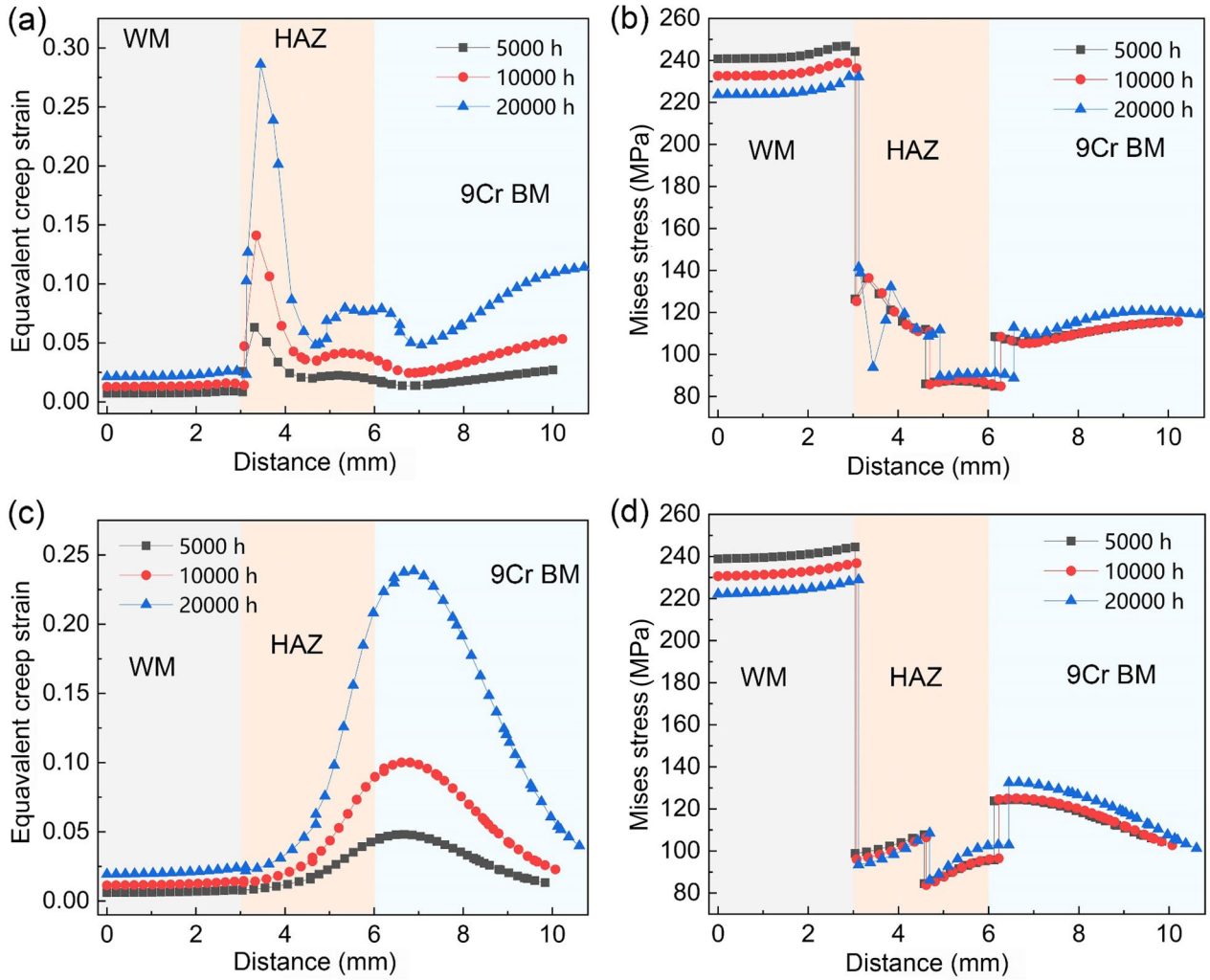

Figure 5 Equivalent creep strain and Mises stress profiles across I-type interface after different creep time: (**a**) and (**b**) Along path 1 in Figure 1(c), (**c**) and (**d**) Along path 2 in Figure 1(c)

equivalent creep strain in the nickel-based WM was minimal due to its good creep resistance. Because the CTE of WM was much higher than that of 9Cr steel, Mises stress in WM was higher than that in 9Cr steel, as shown Figure 5(b). Meanwhile, the Mises stress at the WM/HAZ interface was highest in the 9Cr steel part consisting of HAZ and BM, as shown Figure 5(b). Under the combination of equivalent creep strain and Mises stress concentrations, it could be inferred that the nickel-based WM/HAZ interface was the most dangerous in the I-type interface joint, easily resulting in cracking. Figure 5(c) shows the change in equivalent creep strain in sample middle from 5000 h to 20000 h in the I-type interface joint. The equivalent creep strain concentration occurred near the interface between HAZ and BM, as shown Figure 5(c), and the strain concentration at this position became more and more serious with the extension of creep time. The stress concentration near the HAZ/BM interface was obvious, as shown Figure 5(d). Under the combination of equivalent creep strain and Mises stress concentrations, Type IV crack might occur around the HAZ/BM interface in the middle of I-type interface joint. It should be noted that the absolute value of stress and strain in the middle of the sample was lower than that near the surface of the sample.

Figure 6(a) and (b) shows the change in equivalent creep strain and Mises stress near sample surface from 5000 h to 37000 h in the double Y-type interface joint. When the creep time was less than 20000 h, the creep strain mainly concentrated near the WM/HAZ interface, and when the creep time was extended to 37000 h, the creep strain concentration position had changed from the WM/HAZ interface to the HAZ/BM interface, as shown in Figure 6(a). Similarly, the position of Mises

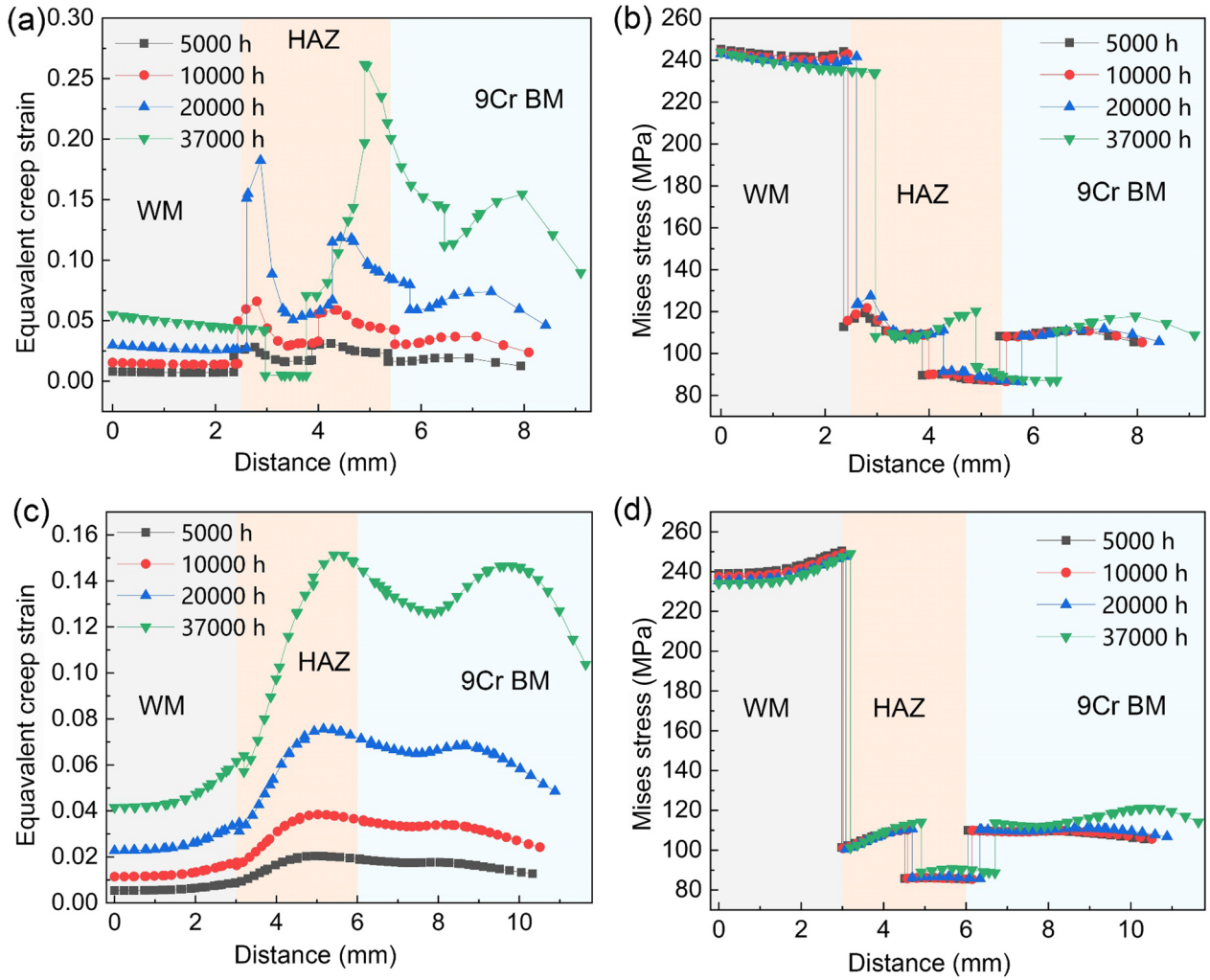

Figure 6 Equivalent creep strain and Mises stress profiles across double Y-type interface after different creep time: (**a**) and (**b**) Along path 1 in Figure 1(d), (**c**) and (**d**) Along path 2 in Figure 1(d)

stress concentration also changed from near the WM/HAZ interface to near the HAZ/BM interface with the extension of creep time, as shown in Figure 6(b). In the middle of double Y-type interface sample, the positions of creep strain concentration appeared near the HAZ/BM interface and in its nearby BM, as shown in Figure 6(c), and the maximum equivalent creep strain in the joint was ~ 15% after 37000 h. When the I-type interface joint was crept for 20000 h, the maximum equivalent creep strain in the middle of the sample had reached 24% (see Figure 5(c)). Thus, the creep strain distribution in the middle of the double Y-type interface sample was more uniform that of the I-type interface sample, which was beneficial to the creep life of the whole joint. In the middle of the double Y-type interface sample, the position of creep strain concentration (see Figure 6(c)) did not coincide with the position of stress concentration (see Figure 6(d)), which was also beneficial to the service safety of the joint. From the perspective of creep strain and stress concentrations, the most vulnerable to failure in the double Y-type interface joint had been changed to the HAZ/BM interface and its nearby BM.

3.2 Micro-Mechanism Analysis of Failure of DMWs with Different Interface Forms by the Combination of Creep Test and Microstructure Characterization

The simulation results in Section 3.1 show that adopting double Y-type interface could shift the creep failure location from the WM/HAZ interface to the HAZ and even the BM. Double Y-type interface prolonged the failure time of the joint and made the joint show a large plastic deformation before failure, which was beneficial to the improvement of the service life of the joint and the failure prediction. In Section 3.2, the DMWs with different

interface forms were fabricated by welding, and the creep tests were carried out to investigate the effect of interface form on the creep behaviors. After creep tests, the microstructures of the crept DMWs were characterized to analyse the micro-mechanism of failure. Meanwhile, the influence of oxidation on the failure of the DMWs was considered by observing the broken sample after creep test. The BMs were 9Cr steel and nickel-based alloy respectively, and the filler metal was Inconel 82 nickel-based wire. Nickel-based alloy was used as one side BM of DMW mainly to avoid the influence caused by the CTE difference between it and WM, and then the research could be focused on the ferritic steel side. TIG welding was used with multilayer technique. The two kinds of WM/ferritic HAZ interface forms were realized by different welding strategies, which were as follows: (1) Butt welding was applied to the BMs without groove, resulting in the approximately I-type interface between WM and 9Cr steel. (2) Butt welding was applied to the BMs without groove, and then a round bar was taken perpendicular to the welding direction. Subsequently, the cap welding was performed along the WM/ferritic HAZ interface on the round bar surface. Finally, the weld reinforcement due to cap welding was removed and the cylindrical creep sample was obtained, which was approximately double Y-type interface between WM and 9Cr steel.

3.2.1 Creep Test Results

The DMW containing I-type interface completely broke and failed after creep for 12744 h, and the DMW containing double Y-type interface completely broke and failed after creep for 13821 h. The failure locations of the above two DMWs were in the ferritic steel side. The creep life of the double Y-type interface DMW was higher 8.5% than that of the I-type interface DMW. In order to analyze the mechanism for the increase of the creep life after applying double Y-type interface, the failure paths of creep samples of DMWs with different interface forms were investigated.

The creep sample containing I-type interface DMW roughly fractured along the nickel-based WM/ferritic HAZ interface. The cross sectional image of the ruptured sample was obtained by OM, and Figure 7 shows the crack path profile of it. The fracture location was mainly at the WM/HAZ interface and in its nearby HAZ. When the crack propagated along the WM/HAZ interface, no obvious macroscopic plastic deformation occurred on both sides. The plastic deformation was large at position (e) in Figure 7(a), meaning that this position suffered the instant tensile fracturing and was final fractured site of the whole sample. Therefore, the failure mode of the I-type interface DMW should be cracking along the WM/HAZ interface and occasionally in the HAZ, and then the crack propagated into the HAZ until complete failure. The failure process was indicated by the white arrows in Figure 7.

Figure 8(a) shows the cross sectional image of the ruptured double Y-type interface DMW by OM, and Figure 8(b) shows the enlarged image near the failure location. The failure of the double Y-type interface DMW mainly occurred in the HAZ, not along the WM/HAZ interface. Interface failure is the most dangerous premature failure mode. Under the same creep testing conditions, the DMW by applying cap welding (approximately double Y-type WM/ferritic HAZ interface) transferred the failure position into the ferritic HAZ. The increase in the creep life of double Y-type interface DMW than

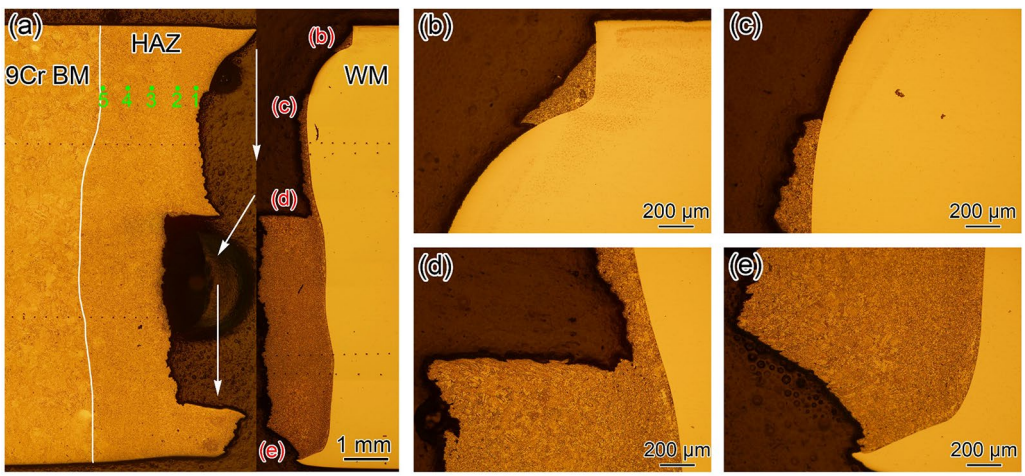

Figure 7 Cross sectional images of the creep sample of ruptured DMW containing I-type interface: (**a**) Overall OM image, (**b**)–(**e**) Detailed OM images

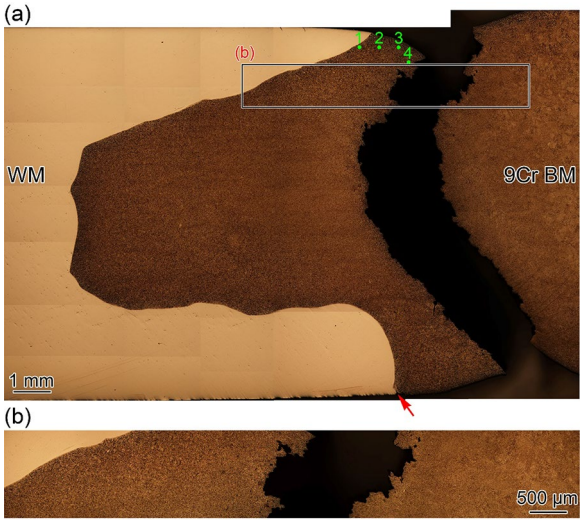

Figure 8 Cross sectional images of the creep sample of ruptured DMW containing double Y-type interface: (**a**) Overall OM image, (**b**) Detailed OM image

that of I-type interface DMW could be attributed to the change of failure mode. Meanwhile, the plastic deformation of the DMW with double Y-type WM/HAZ interface was large after creep, which was also beneficial to the failure monitoring. The result of creep tests that double Y-type interface DMW had longer life and the failure location of it was in ferritic HAZ was consistent with that of the FEA simulation in Section 3.1.

3.2.2 The Failure Mechanism of DMW Containing I-type Nickel-Based WM/Ferritic HAZ Interface

To reveal micro-mechanism of failure, microstructure and chemical composition of the ruptured sample were characterized after creep. Figure 9 shows microstructures and O element distribution at the position (d) in Figure 7(a). Oxide notch was formed along the nickel-based WM/ferritic HAZ interface, as shown in Figure 9(a). Figure 9(b) shows the O elemental map corresponding to Figure 9(a), in which O-rich area was the oxide notch. Oxide notch was the precursor of interface failure of DMW and promoted interface cracking [50]. Meanwhile, it is worth noting that there had been interfacial oxidation in front of the tip of oxide notch, as marked by the white circle in Figure 9(b). During long term high temperature exposure, a band of ultra-fine ferrite grain would form along the interface between nickel-based WM and ferritic HAZ, and the grain boundaries of ultra-fine ferrite could act as oxygen diffusion channels to make oxidation occur along the interface [40]. As expected, there was ultra-fine ferrite grain formed along the nickel-based WM/ferritic HAZ interface in this study, as indicated by the yellow arrows in Figure 9(d). The hardness of ultra-fine ferrite at the interface was significantly lower than that of the microstructures on both sides [39], and thus the interfacial ultra-fine ferrite was inclined to be deformed. Some researches [54, 55] have pointed out that the uncoordinated deformation on both sides of the interface would lead to the shear stress and thus the interfacial stress concentration. It could be inferred that there should be serious shear stress and stress concentration near the WM/HAZ interface due to the formation of interfacial ultra-fine ferrite (see the microstructure marked by yellow arrows in Figure 9(d)), leading to creep cracking along the WM/HAZ interface, as indicated by the red arrows in Figure 9(c). Hence, interface failure of the DMW containing I-type interface was the combined result of interface oxidation and interface cracking.

The failure path of the crept DMW containing I-type interface occasionally entered the HAZ near the interface, as shown in Figure 7(b) and (c). Further observation by SEM shows that these locations were in CGHAZ and fine-grained heat-affected zone (FGHAZ), as shown in Figure 10. A large number of creep voids were observed in CGHAZ near the failure path, as shown in Figure 10(a), (b). Lots of creep voids were also observed in the FGHAZ near the failure path, as shown in Figure 10c. Therefore, the cracking in the HAZ was related to the formation of creep voids. It was further that the creep voids and micro-cracks in the FGHAZ were mainly generated at the fine grain boundaries, as shown in Figure 10(d).

The microstructure near the failure path of the ruptured DMW containing I-type interface was observed by EBSD, and the results are shown in Figure 11. Inverse pole figure (IPF) + image quality (IQ) map clearly shows the creep voids formed along the coarse grain boundaries and fine grain boundaries in the HAZ, as indicated by the white arrows in Figure 11, and the trace of the creep voids connecting to form main crack could be seen on the failure path. Researchers obtained crystal misorientation data by EBSD and found that some characteristic parameters reflected deformation and damage, in which Grain Reference Orientation Debiation (GROD) could represent the deformation ability of grains. Kobayashi et al. [56] and Rui et al. [57] pointed out that GROD has a good linear relationship with creep deformation. GROD + IQ map in Figure 11 indicates that there was obvious creep deformation in the entire HAZ, and thus creep voids and cracking preferentially formed around the grain boundaries in the HAZ. According to the above experimental observation and analysis, the failure of crept DMW containing I-type interface was related to the cracking of the interfacial ultra-fine ferrite and the creep voids formed around the grain boundaries in CGHAZ and FGHAZ.

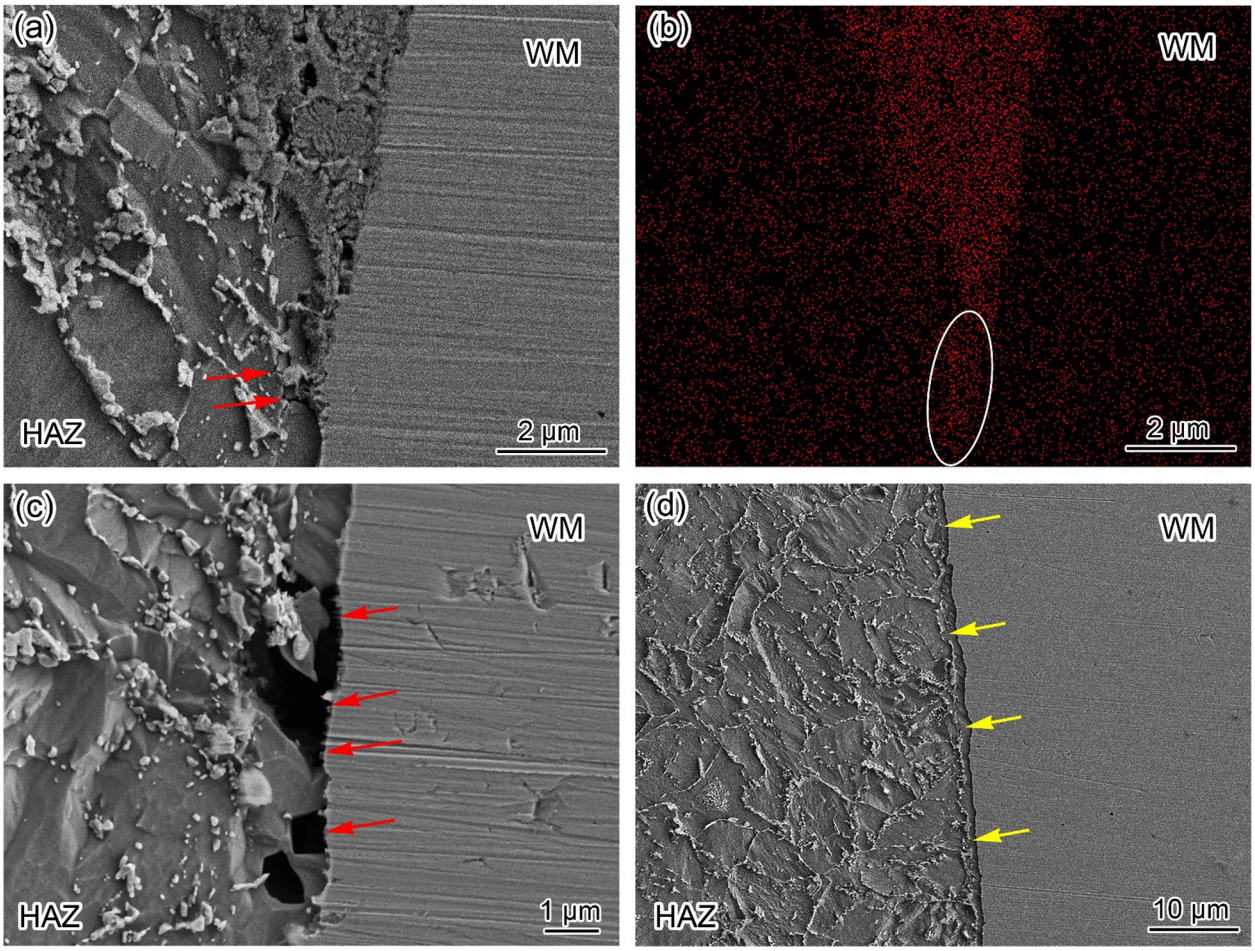

Figure 9 Microstructures and O element distribution near the nickel-based WM/ferritic HAZ interface of the I-type interface DMW after 600 ℃/140 MPa creep test: (**a**) SEM image of interface oxide notch, (**b**) O elemental map, corresponded to (**a**), (**c**) Interface crack, (**d**) Ultra-fine ferrite band along the interface

Based on the above experimental results, the creep failure micro-mechanism of the DMW containing I-type interface was clarified. The interfacial oxide notch triggered the fracture along the WM/ferritic HAZ interface. The interfacial ultra-fine ferrite formed during creep was inclined to be cracking, resulting in crack propagation along the WM/ferritic HAZ interface. Meanwhile, a large number of creep voids were formed around the grain boundaries in the CGHAZ and FGHAZ, and crack could also propagate into the CGHAZ and FGHAZ.

3.2.3 The Failure Mechanism of DMW Containing Double Y-type Nickel-Based WM/Ferritic HAZ Interface

The result of creep tests shows that the failure location of the DMW containing double Y-type interface was mainly in ferritic HAZ, as shown in Figure 8. The microstructures on the failure path were observed by SEM to obtain more failure information. Figure 12 shows SEM images of the failure path in the HAZ, and the microstructure indicated that this area was ICHAZ. A large number of creep voids were observed near the crack, as indicated by the black arrows in Figure 12(a), (b). EBSD was performed to further analyze the microstructure of the failure path, and the results are shown in Figure 13, which directly shows that the failure occurred in the ICHAZ composed of fine grains. Figure 12(c) shows the connection of creep voids, and similar results could be found in Figure 13(b). In addition, a large number of micro-cracks and voids were observed on the fine-grain boundary without precipitated phase in the ICHAZ, as shown in Figure 12(d). The above experimental evidence directly indicated that the failure process began with the formation of a large number of creep voids and micro-cracks in ICHAZ, and then creep voids and micro-cracks continued to grow and connect with each other, eventually leading to cracking. Thus, the failure of the DMW containing double Y-type interface was related with the Type IV fracture in HAZ. Type IV fracture in ferritic HAZ

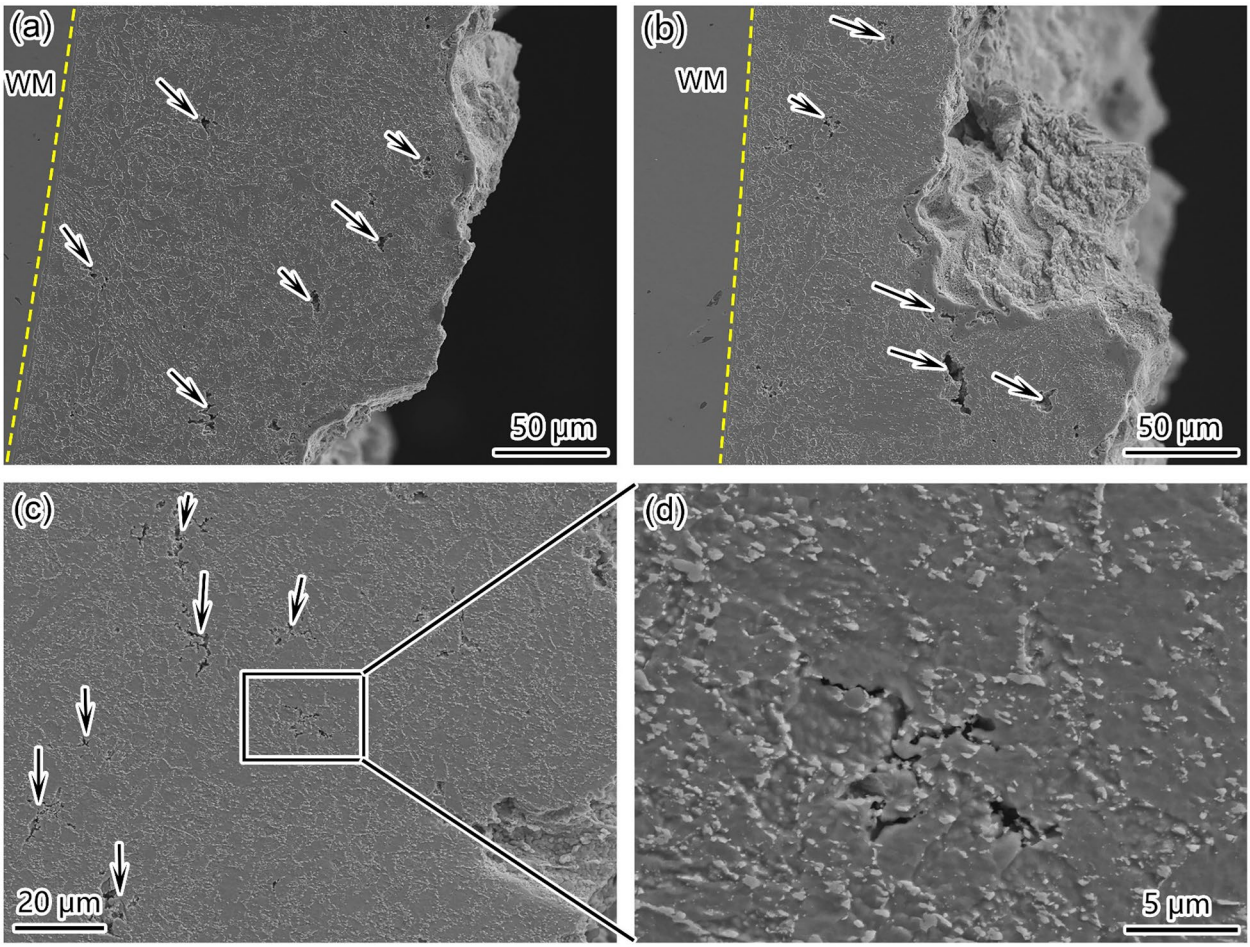

Figure 10 SEM images near the fracture path of the I-type interface DMW after 600 ℃/140 MPa creep test: (**a**) and (**b**) CGHAZ near the interface, (**c**) and (**d**) FGHAZ near the interface

was a typical creep failure mode of the joints containing 9%–12%Cr martensitic heat-resistant steels. The common causes of Type IV fracture were matrix softening, precipitate coarsening and lack of precipitate pinning at grain boundaries [18–23]. The failure mechanism of the DMW containing double Y-type interface will be investigated below.

In order to determine the micro-mechanism of Type IV fracture in ICHAZ of the DMW containing double Y-type interface, the characteristics of hardness and microstructure of HAZ should be clarified first. Figure 14 shows hardness profiles across the nickel-based WM/ferritic HAZ interface of DMW before and after creep test. Before the creep test, the hardness of HAZ was higher than that of WM and BM. Furthermore, the hardness decreased in the HAZ with increasing distance from WM/HAZ interface. The microstructures in the HAZ would undergo different phase transformations during welding heating and subsequent cooling, so the HAZ could be further divided into CGHAZ, FGHAZ and ICHAZ as increasing distance from WM/HAZ interface. The CGHAZ adjacent to the interface had the highest hardness, as shown in Figure 14. The microstructure in FGHAZ was completely austenitized during welding heating and fine martensite was formed after cooling, and the hardness of FGHAZ was high due to the presence of a large number of fine grain boundaries. Only part of the microstructure in ICHAZ was austenitized during welding heating, and the ICHAZ after cooling contained both the newly formed quenched martensite and the prior martensite. Thus, the hardness of ICHAG was low than that of FGHAZ, and there was a hardness valley in the HAZ before creep test, as shown in Figure 14. After the creep test, the hardness of WM increased and the hardness of the HAZ decreased. In addition, the hardness of ICHAZ was still the lowest after the creep test. It has been reported that the hardness of martensite steel would decrease due to the microstructure degradation

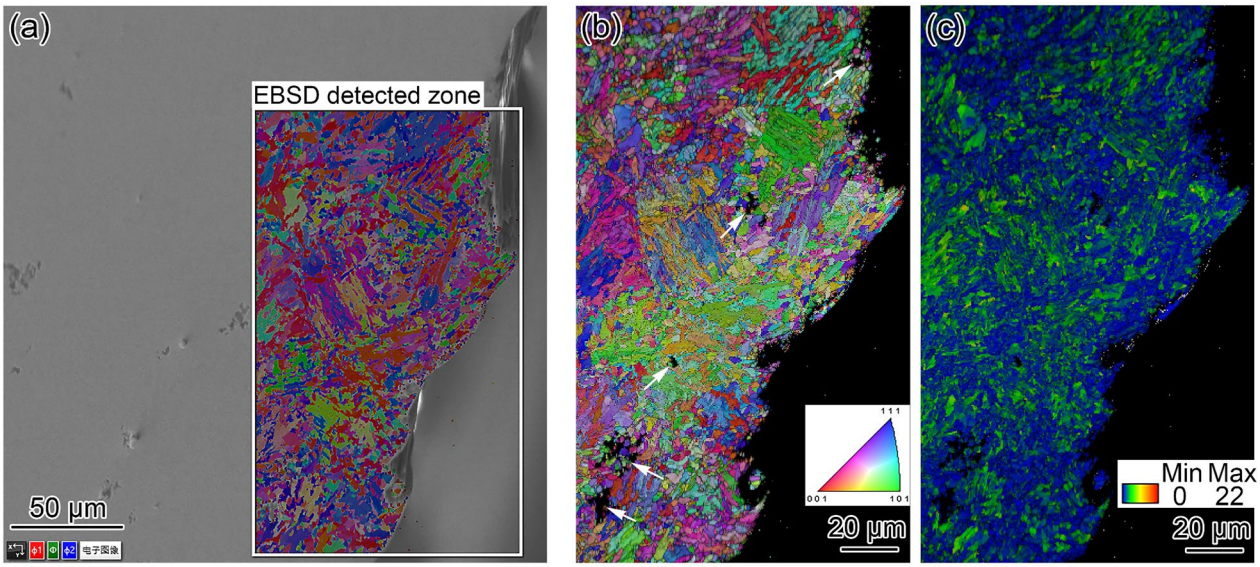

Figure 11 EBSD images near the fracture path of the I-type interface DMW after 600 ℃/140 MPa creep test: (**a**) Detected zone, (**b**) IPF + IQ map, (**c**) GROD + IQ map

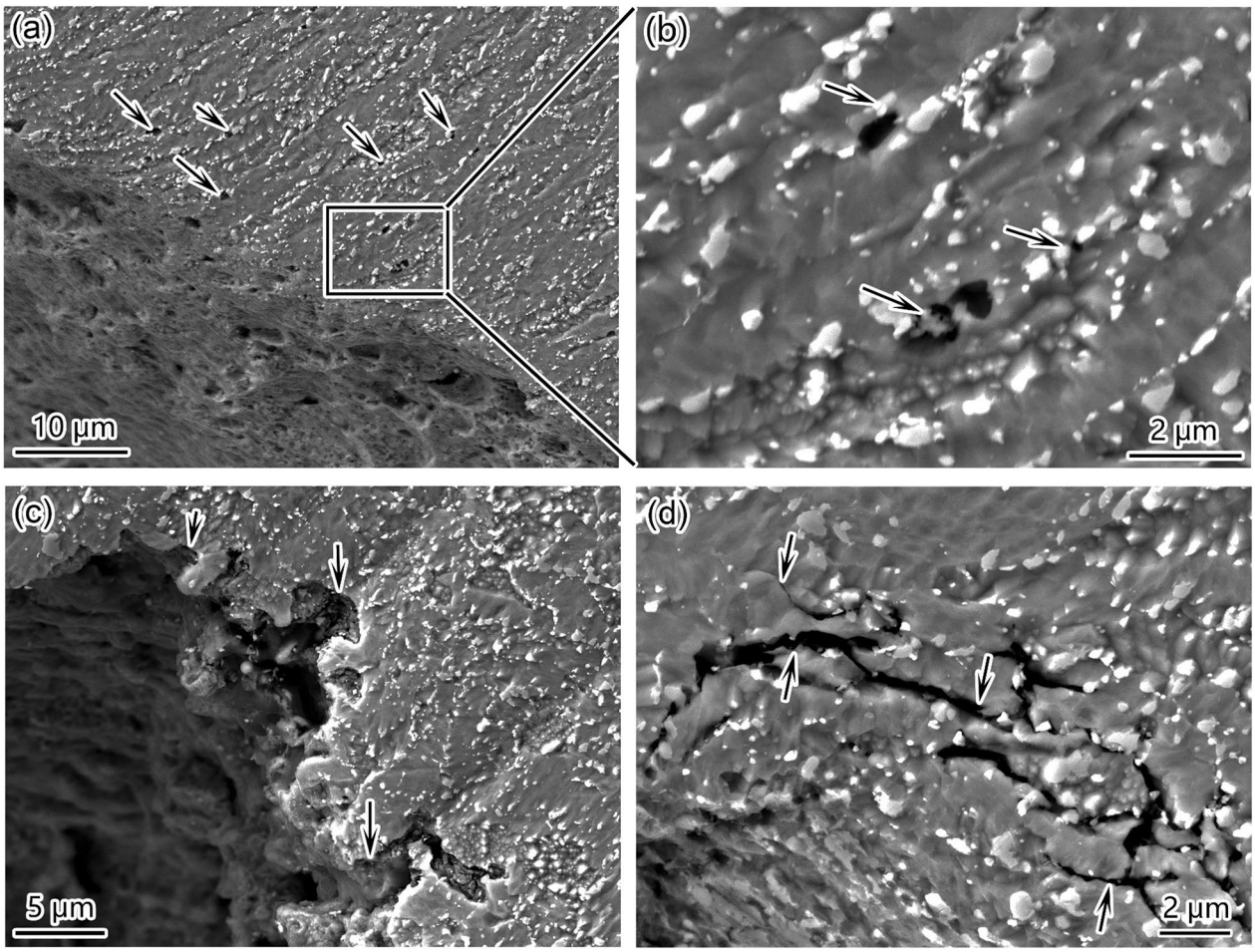

Figure 12 SEM images near the fracture path of the double Y-type interface DMW after 600 ℃/140 MPa creep test

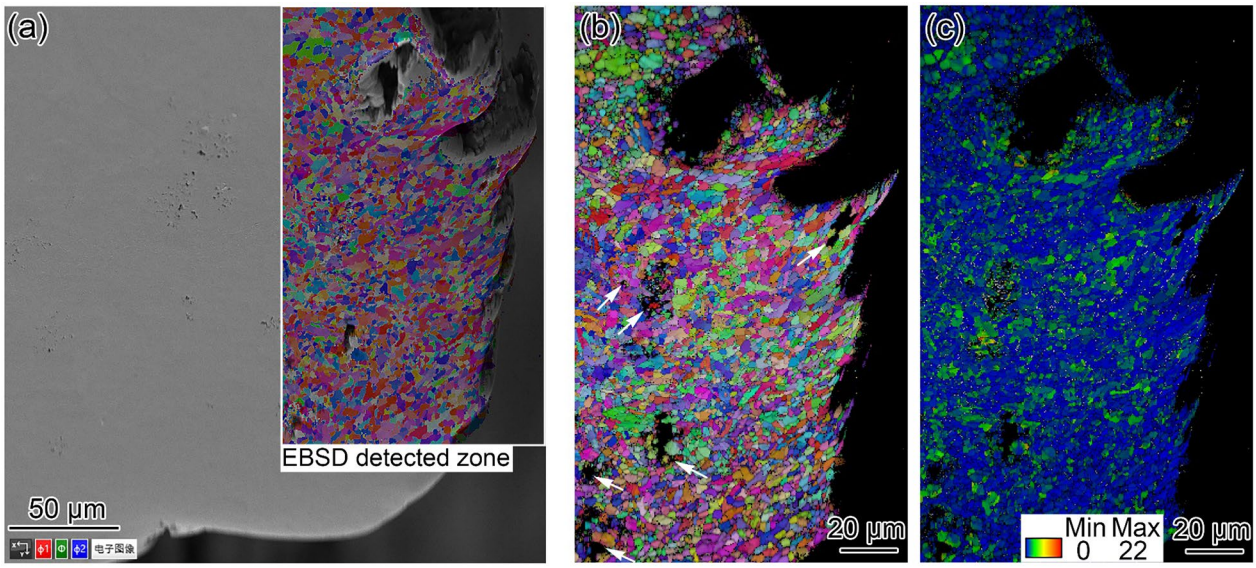

Figure 13 EBSD images near the fracture path of the double Y-type interface DMW after 600 ℃/140 MPa creep test: (**a**) Detected zone, (**b**) IPF + IQ map, (**c**) GROD + IQ map

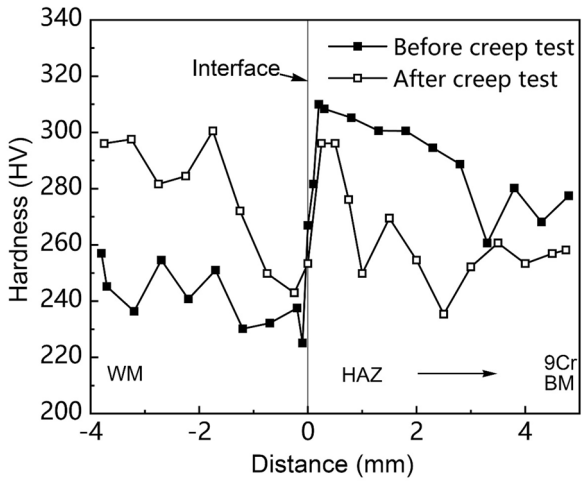

Figure 14 Hardness profiles of the 9Cr steel side in DMW before and after creep test at 600 C/140 MPa

and the recovery softening during creep process [26, 27], and in this study the softening behavior also occurred in the HAZ of 9Cr steel. Laha et al. [27] found that the hardness of nickel-based WM increased during the creep process, and they believed that it was related to the precipitation hardening behavior in WM. Zhang et al. [43] provided direct experimental evidence for the above viewpoint. Zhang et al. [43] noted that the precipitates in the nickel-based WM were mainly distributed at the solidified sub-grain boundaries with a small amount of them in interior of grains before creep, while a large number of dispersed precipitates appeared in interior of grains in the WM after creep, which strengthened the WM and increased the hardness of the WM after long term creep. It explained the increase in WM hardness after creep in this study.

In the ICHAZ, the formation of a large number of fine-grain boundaries without precipitated phase pinning was related to the microstructure evolution during welding thermal cycle. Figure 15(a) shows the matrix microstructures of the 9Cr steel BM. There were lots of precipitated phases on the prior austenite grain boundaries and martensitic lath boundaries, as shown in Figure 15(a). During the welding heating process, the peak temperature in the ICHAZ was higher than A_{c1} and lower than A_{c3}, which caused part of the matrix microstructure to be re-austenitized. The welding heating process was extremely fast and thus the newly formed austenite cannot grow, and a large number of fine grains were formed after cooling. Meanwhile, the precipitated phases in the ICHAZ were only partially dissolved during welding heating and the alloying elements were not much dissolved back into the matrix, which meant that there would not be lots of precipitated phases formed on the newly formed fine-grain boundaries in the ICHAZ due to lack of sufficient alloying elements. As a result, a large number of fine-grain boundaries without precipitated phase pinning were formed in the ICHAZ, as shown in Figure 15(b).

The results in Figure 14 show that ICHAZ was a low hardness region in the HAZ, and the softening behavior of matrix in ICHAZ was also the most serious in the creep process. Meanwhile, the simulation results in Section 3.1 show that there would be the

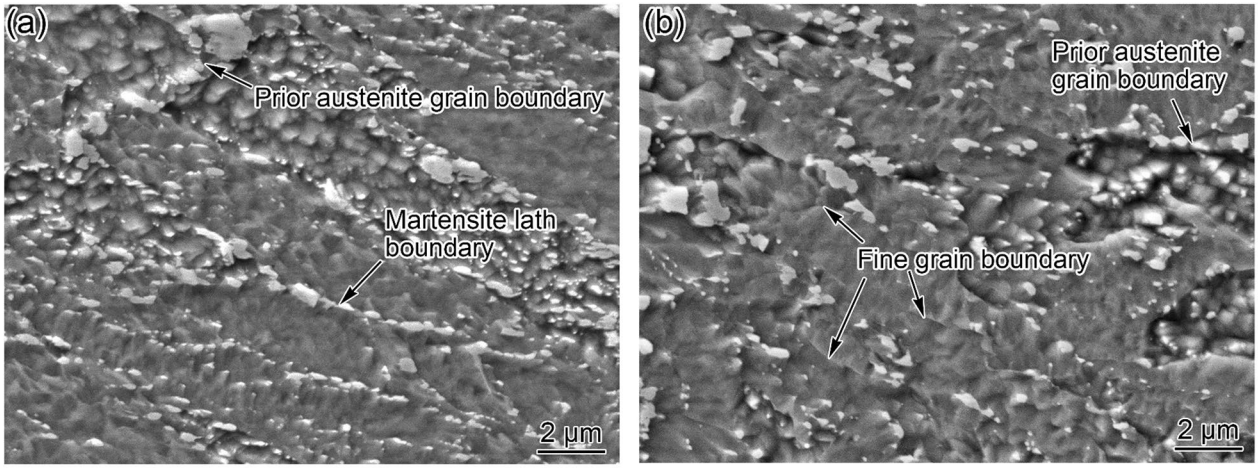

Figure 15 SEM images of microstructures of 9Cr steel BM and its ICHAZ: (**a**) BM, (**b**) ICHAZ

creep strain concentration in the ICHAZ of the double Y-type interface DMW in the creep process. On the one hand, it would lead to the uncoordinated deformation between the matrix and precipitated phase in ICHAZ, which aggravated the stress concentration at the boundary between the matrix and the precipitated phase, promoting the formation of creep void around the precipitated phase. The SEM image in Figure 12(b) shows that the creep voids formed around the precipitated phases, which indicated the critical role of matrix softening in the formation of the creep void in the ICHAZ. On other hand, creep deformation of the fine grains in ICHAZ (see GROD result in Figure 13(c)) was high, and the fine-grain boundaries without precipitated phase pinning would slip during creep, resulting in the micro-cracks on the fine-grain boundaries (see Figure 12(d)). In this study, precipitated phases in the ICHAZ did not grow significantly during creep process, and the creep voids in Figure 12(b) did not all initiate around the precipitates with larger size, so precipitate coarsening was not the main reason for Type IV fracture in the DMW containing double Y-type interface.

In addition, the oxidation along the WM/ferritic HAZ interface in the double Y-type interface DMW was observed by SEM, which corresponded to the position indicated by red arrow in Figure 8(a), and the results are shown in Figure 16. Although there was oxide notch and crack along the WM/ferritic HAZ interface on the sample surface, interface failure was not triggered, which proved that the double Y-type interface form could suppress the promoting effect of oxide notch on interface failure.

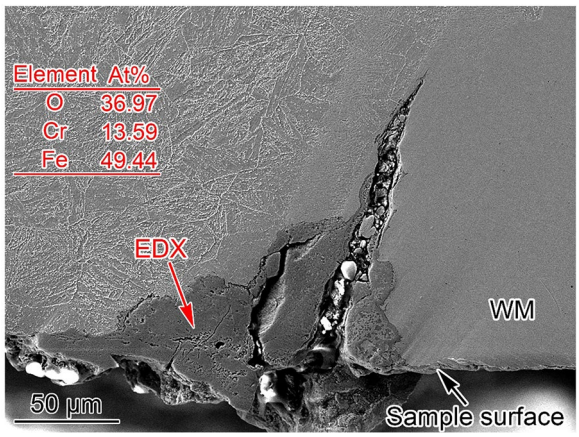

Figure 16 Interfacial oxidation of the double Y-type interface DMW after 600 ℃/140 MPa creep test, corresponed to the position marked by red arrow in Figure 8(a)

3.3 Creep Damage and Life Analyses of DMWs with Different Interface Forms

In order to further analyse the creep life of I-type interface DMW (butt welding without groove) and double Y-type interface DMW (application the cap welding at the interface), the creep damage of the two kinds of DMWs was quantitatively compared. $\overline{\text{GROD}}$ has the linear relationship with creep deformation [56, 57], which was used as an indicator of creep damage in this study. $\overline{\text{GROD}}$ near the creep failure path of two kinds of DMWs was obtained by EBSD. Starting from the failure location, EBSD was performed at a certain distance to obtain a serious of GROD maps perpendicular to the failure path. The detected zone of EBSD was 150 μm × 150 μm and the step size of it was 0.4 μm. 140625 pixels were obtained in each detected zone. The GROD data corresponding to each pixel was extracted. The $\overline{\text{GROD}}$

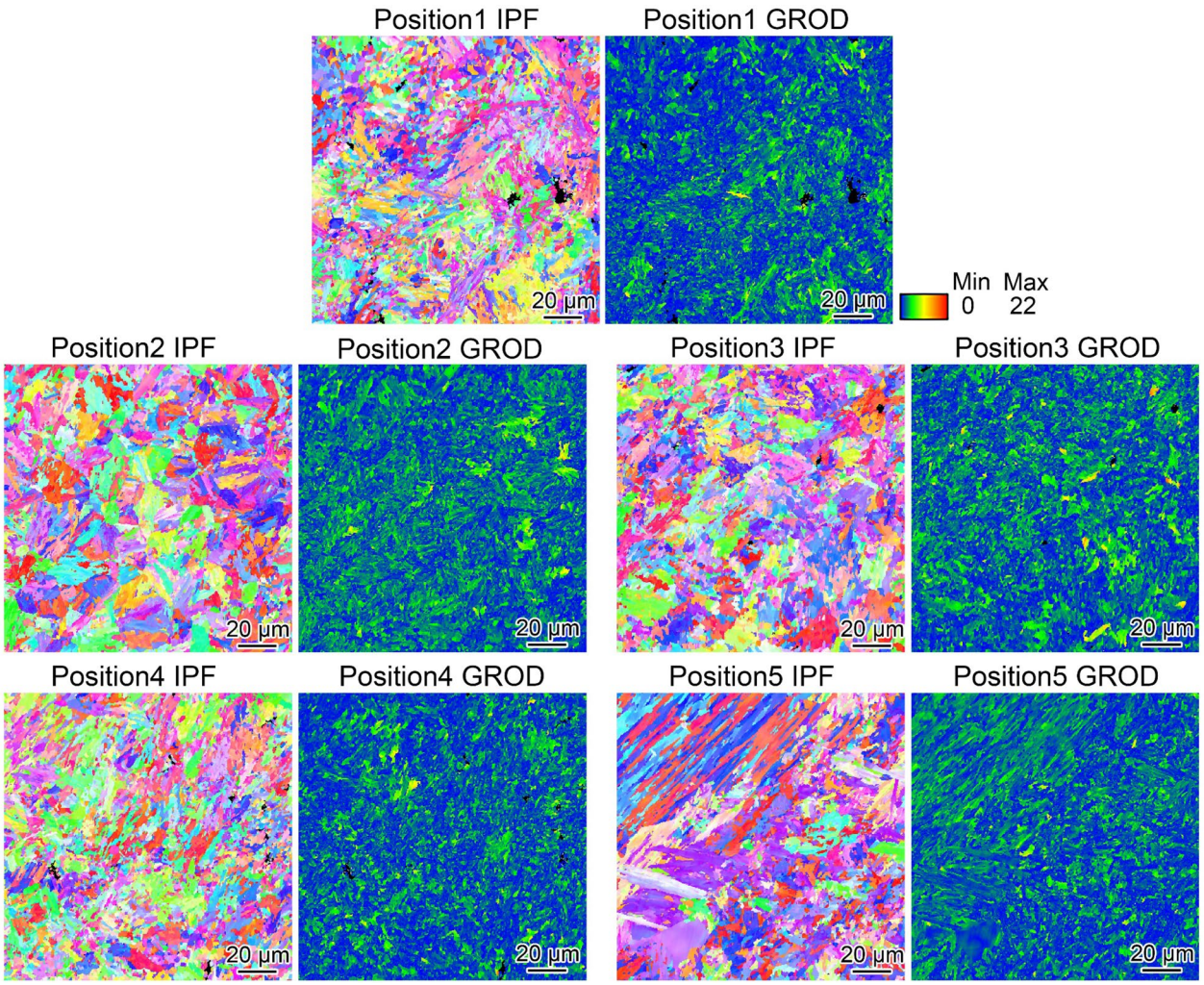

Figure 17 IPF maps and corresponding GROD maps in the ruptured I-type interface DMW after 600 ℃/140 MPa creep test (Positions 1–5 were illustrated in Figure 7(a))

was calculated for each EBSD detected zone as the following equation:

$$\overline{\mathrm{GROD}} = \frac{1}{140625}\sum_{m-1}^{375}\sum_{m-1}^{375}\mathrm{GROD}\ (m,n). \tag{1}$$

Figure 17 shows the IPF maps and corresponding GROD maps in the ruptured DMW without groove after 600 ℃/140 MPa creep test. Five positions were detected zones, which were marked by the green dots and numbered by 1–5, as shown in Figure 7(a). According to the grain size characteristic in IPF map in Figure 17, position 1 was in the CGHAZ. Fine grains appeared at position 2, which meant that position 2 began to enter the FCHAZ. It gradually entered ICHAZ from position 3 to position 4. Position 5 was the boundary between the HAZ and BM. GROD in position 1 to position 5 first increased and then decreased. The $\overline{\mathrm{GROD}}$ of above five positions was calculated respectively, which was plotted in Figure 18 with

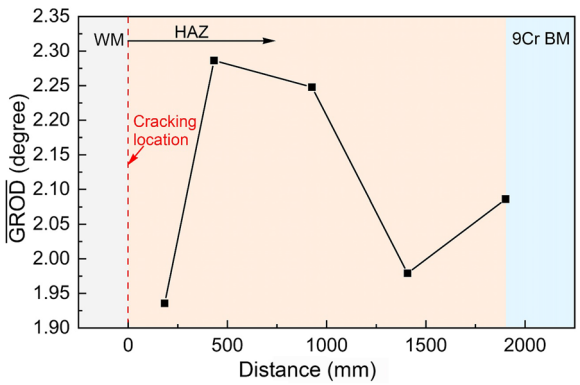

Figure 18 $\overline{\mathrm{GROD}}$ profile near the failure path of the ruptured I-type interface DMW after 600 ℃/140 MPa creep test

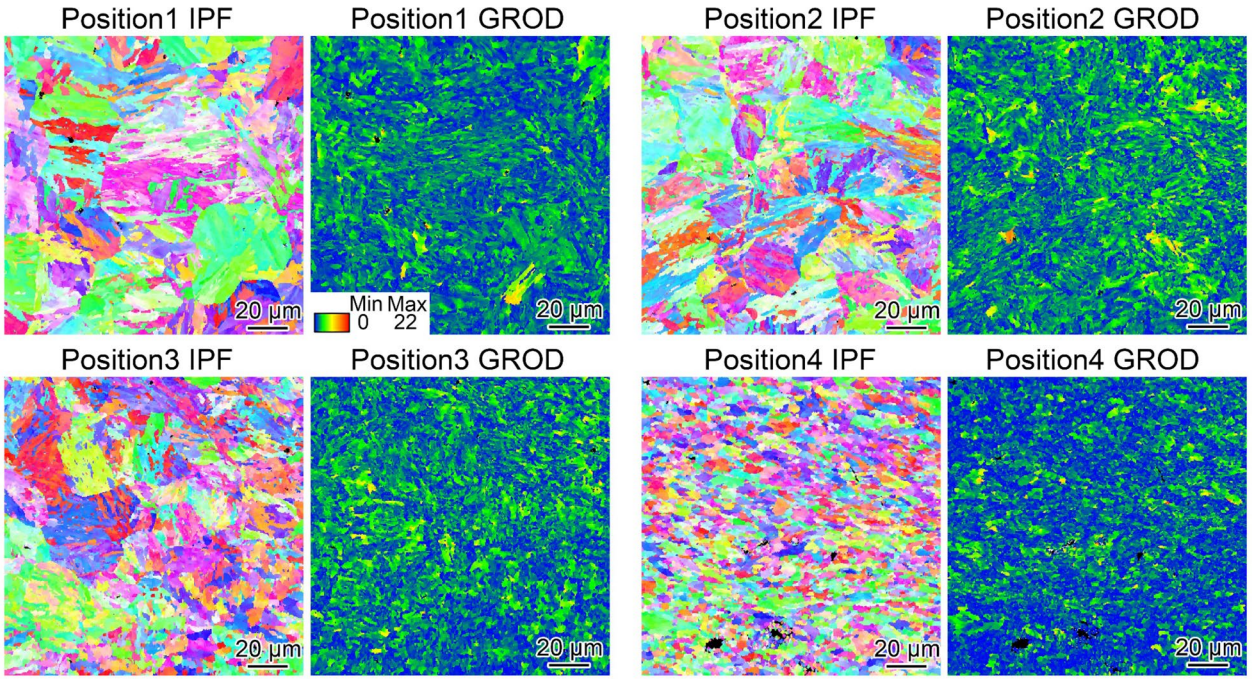

Figure 19 IPF maps and corresponding GROD maps in the ruptured double Y-type interface DMW after 600 ℃/140 MPa creep test (Positions 1–4 were illustrated in Figure 8(a))

the distance as the horizontal coordinate. The variation trend of creep damage from WM/HAZ interface (also the failure location) to BM was obtained. There were creep voids with a large size in the HAZ near WM/HAZ interface (position 1 in Figure 17). However, the $\overline{\text{GROD}}$ of position 1 was not high (see Figure 18) and the failure occurred along the WM/HAZ interface instead of at the position 1, which meant that the interfacial ultra-fine ferrite was more prone to cracking and was more dangerous degraded microstructure. In addition, there were creep voids around the grain boundaries at position 1 (see Figure 17) and the $\overline{\text{GROD}}$ in the HAZ near the WM/HAZ interface was high (see Figure 18), which was also consistent with the result that crack occasionally entered HAZ (see Figure 10). The above results show that the WM/HAZ interface and the CGHAZ/FGHAZ near the interface were the weak positions of the I-type interface DMW.

Figure 19 shows the IPF maps and corresponding GROD maps in the ruptured DMW with cap welding after 600 ℃/140 MPa creep test. Four positions were detected zones, which were marked by the green dots and numbered by 1–4 in Figure 8(a). Position 1 in Figure 19 was in the CGHAZ with few creep voids. There was a gradual transition to the FGHAZ from position 2 to position 3. Position 4 was in the ICHAZ with a significant increase in the number of creep voids, which was consistent with the occurrence of Type IV crack in ICHAZ of the double Y-type interface DMW. The $\overline{\text{GROD}}$ of above four positions was calculated respectively, which was plotted in Figure 20 with the distance as the horizontal coordinate. The creep damage variation trend from the WM/HAZ interface to the ICHAZ in the double Y-type DMW was obtained (see Figure 20), which was basically consistent with that in the I-type DMW (see Figure 18), but the failure locations of two kinds of DMWs were different, which was related to the change of interface form. On the one hand, the angle between the nickel-based WM/ferritic HAZ interface and the external load was

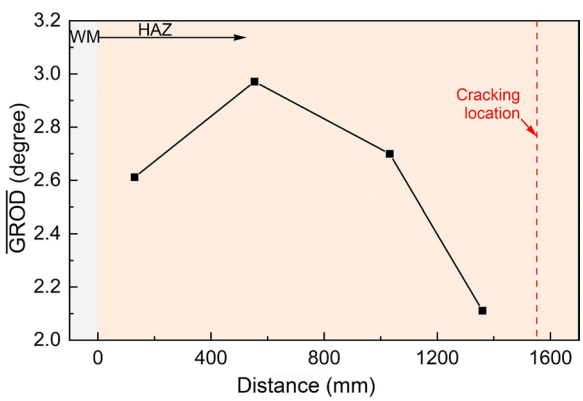

Figure 20 $\overline{\text{GROD}}$ profile near the failure path of the ruptured double Y-type interface DMW after 600 ℃/140 MPa creep test

about 30° in the DMW with cap welding, which made the stress component of the external load of 140 MPa at the vertical interface only 70 MPa. Therefore, the interfacial ultra-fine ferrite was not cracking during the creep process, which prevented the interface failure. On the other hand, according to the simulation results in Section 3.1, even if there was interfacial oxide notch, the double Y-type interface form could avoid a large range of stress concentration near the WM/HAZ interface to a certain extent, which was also one of the reasons why application of cap welding could lead the failure location from the WM/HAZ interface to the ICHAZ and even BM.

According to the simulation results in Section 3.1, changing the interface form from I-type to double Y-type could shift the stress and strain distributions and transfer the creep strain concentration from the WM/ferritic HAZ interface into the ferritic HAZ and even to the ferritic BM, which was from the mechanical view to prolong creep life of the DMW. The comparison experiment in Section 3.2 took into account the evolution of microstructure and the existence of oxidation. In this case, there were both the interfacial ultra-fine ferrite band that was prone to crack and the interfacial oxide notch, which was a coupling effect of microstructure degradation and oxidation damage along the WM/HAZ interface. Based on the results in Sections 3.1 and 3.2, it is known that creep strain concentration could be separated from the WM/ferritic HAZ interface after application of double Y-type interface form, and thus it was decoupled from the interfacial microstructure degradation and the interfacial oxidation, which was beneficial to avoid interface cracking and prolong life of the DMW.

4 Conclusions

In this study, the creep behaviors of the DMWs involving different forms of interface between nickel-based WM and ferritic heat resistant steel BM were investigated by means of numerical simulation and experimental methods. The effects of conventional I-type interface form and novel double Y-type interface form on creep failure mechanism and life of DMW were clarified. The main conclusions are as follows:

(1) For the DMW containing I-type interface between WM and BM, creep failure would occur near the WM/HAZ interface. While changing the WM/HAZ interface form from I-type to double Y-type, the creep failure occurred in the HAZ or even in the BM. The creep life of the double Y-type interface DMW was longer than that of the I-type interface DMW, which was related to the shift of failure position and thus the avoidance of interface premature failure.

(2) For the I-type interface DMW, there was strain concentration and ultra-fine ferrite band at the interface during long term creep, as well as interfacial oxide notch, inducing the failure around WM/HAZ interface. Oxide notch triggered cracking along the interface. Strain concentration and ultra-fine ferrite band led to the uncoordinated deformation at the interface, inducing interfacial stress concentration, and then the creep voids were formed along the interface and in the CGHAZ/FGHAZ near it. The interface premature failure was the result of strain/stress concentration, microstructure degradation and oxidation coupling acting on the interface.

(3) In the double Y-type interface DMW, creep strain concentrated near the HAZ/BM interface, instead of near the WM/HAZ interface. The triggering effect of oxide notch on interface failure also failed for the double Y-type interface DMW. By applying double Y-type interface form in DMW, strain/stress concentration, microstructure degradation and oxidation had been decoupled from the WM/HAZ interface. The creep failure of the double Y-type interface DMW was caused by Type IV crack in the ICHAZ, originating from creep voids and microcracks on fine-grain boundaries, which was related to the matrix softening and the lack of precipitate pinning at fine-grain boundaries in the ICHAZ.

(4) The results of this study suggest the effect of interface form on failure mechanism should be considered to prolong creep life of DMW.

Acknowledgements
Not applicable.

Authors' Contributions
XL wrote the manuscript; XL and JN were in charge of the whole trial; XW KL and HZ assisted with sampling and laboratory analyses. All authors read and approved the final manuscript.

Funding
Supported by Youth Elite Project of CNNC and Modular HTGR Super-critical Power Generation Technology Collaborative Project between CNNC and Tsinghua University Project of China (Grant No. ZHJTIZYFGWD20201).

Data availability
Not applicable.

Declarations

Competing interests
The authors declare no competing financial interests.

Received: 4 January 2024 Revised: 1 February 2024 Accepted: 5 February 2024
Published online: 01 March 2024

References

[1] F Masuyama. History of power plants and progress in heat resistant steels. *ISIJ Int.*, 2001, 41(6): 612-625.

[2] R Viswanathan, J F Henry, J Tanzosh, et al. U.S. program on materials technology for ultra-supercritical coal power plants. *J. Mater. Eng. Perform.*, 2005, 14: 281-292.

[3] R Viswanathan, W Bakker. Materials for ultrasupercritical coal power plants — Boiler materials: Part 1. *J. Mater. Eng. Perform.*, 2001, 10(1): 81-95.

[4] R Viswanathan, J Saver, J M Tanzosh. Boiler materials for ultra-supercritical coal power plants — steamside oxidation. *J. Mater. Eng. Perform.*, 2006, 15(3): 255-274.

[5] J C Vaillant, B Vandenberghe, B Hahn, et al. T/P23, 24, 911 and 92: New grades for advanced coal-fired power plants — Properties and experience. *Int. J. Pres. Ves. Pip.*, 2008, 85(1-2): 38-46.

[6] F Abe. Progress in creep-resistant steels for high efficiency coal-fired power plants. *J. Press. Vess-T. ASME*, 2016, 138(4): 040804.

[7] J N DuPont. Microstructural evolution and high temperature failure of ferritic to austenitic dissimilar welds. *Int. Mater. Rev.*, 2013, 57(4): 208–234.

[8] X Li, K Li, Z Cai, et al. A review of austenite memory effect in HAZ of B con-taining 9% Cr martensitic heat resistant steel. *Metals*, 2019, 9(11): 1233.

[9] J D Parker, G C Stratford. Review of factors affecting condition assessment of nickel based transition joints. *Sci. Technol. Weld. Joi.*, 1999, 4: 29-39.

[10] R D Nicholson. Creep rupture properties of nickel-base transition joints after long-term service. *Mater. Sci. Technol.*, 1986, 2(7): 686–692.

[11] R D Nicholson. Effect of aging on interfacial structures of nickel-based transition joints. *Metals Technol.*, 1984, 11: 115-124.

[12] K Y Shin, J W Lee, J M Han, et al. Transition of creep damage region in dissimilar welds between Inconel 740H Ni-based superalloy and P92 ferritic/martensitic steel. *Mater. Char.*, 2018, 139: 144-152.

[13] M Tabuchi, H Hongo, F Abe. Creep strength of dissimilar welded joints using high B-9Cr steel for advanced USC boiler. *Metall. Mater. Trans. A*, 2014, 45(11): 5068–5075.

[14] H Nomoto. Development in materials for ultra-supercritical (USC) and advanced ultra-supercritical (A-USC) steam turbines. *Advances in Steam Turbines for Modern Power Plants*, 2017: 263–278.

[15] R Viswanathan, K Coleman, U Rao. Materials for ultra-supercritical coal-fired power plant boilers. *Int. J. Press. Vessel. Pip.*, 2006, 83 (11): 778-783.

[16] D I Roberts, R H Ryder, R Viswanathan. Performance of dissimilar welds in service. *J. Press. Vess-T. ASME*, 1985, 107(3): 247-254.

[17] Y Zhang, K J Li, Z P Cai, et al. Creep rupture properties of dissimilar metal weld between Inconel 617B and modified 9%Cr martensitic steel. *Mater. Sci. Eng. A*, 2019, 764: 138185.

[18] D J Abson, J S Rothwell. Review of type IV cracking of weldments in 9–12%Cr creep strength enhanced ferritic steels. *Int. Mater. Rev.*, 2013, 58 (8): 437-473.

[19] L Falat, M Svoboda, A Výrostková, et al. Microstructure and creep characteristics of dissimilar T91/TP316H martensitic/austenitic welded joint with Ni-based weld metal. *Mater. Char.*, 2012, 72: 15-23.

[20] J S Lee, K Maruyama. Mechanism of microstructural deterioration preceding type IV failure in weldment of Mod.9Cr-1Mo steel. *Met. Mater. Int.*, 2015, 21 (4): 639-645.

[21] Y Liu, S Tsukamoto, T Shirane, et al. Formation mechanism of type IV failure in high Cr ferritic heat-resistant steel-welded joint. *Metall. Mater. Trans. A*, 2013, 44 (10): 4626-4633.

[22] K Laha, K S Chandravathi, P Parameswaran, et al. Characterization of microstructures across the heat-affected zone of the modified 9Cr-1Mo weld joint to understand its role in promoting type IV cracking. *Metall. Mater. Trans. A*, 2017, 38 (1): 58-68.

[23] J A Francis, W Mazur, H K D H Bhadeshia. Review type IV cracking in ferritic power plant steels. *Mater. Sci. Tech-Lond*, 2006: 1387–1395.

[24] F Abe, M Tabuchi, S Tsukamoto, et al. Microstructure evolution in HAZ and suppression of Type IV fracture in advanced ferritic power plant steels. *Int. J. Press. Vessel. Pip.*, 2010, 87 (11): 598-604.

[25] C Pandey, M M. Mahapatra, P. Kumar, et al. Effect of post weld heat treatments on microstructure evolution and type IV cracking behavior of the P91 steel welds joint. *J. Mater. Process., Technol.*, 2019, 266: 140–154.

[26] T Matsunaga, H Hongo, M Tabuchi. Interfacial failure in dissimilar weld joint of high boron 9% chromium steel and nickel-based alloy under high-temperature creep condition. *Mater. Sci. Eng. A*, 2017, 695: 302-308.

[27] K Laha, K S Chandravathi, P Parameswaran, et al. A comparison of creep rupture strength of ferritic/austenitic dissimilar weld joints of different frades of Cr-Mo ferritic steels. *Metall. Mater. Trans. A*, 2013, 43: 1174-1186.

[28] B Dooley, P S Chang. The current state of boiler tube failures in fossil plants. *Power Plant Chem.*, 2000, 2.

[29] L F Zhao, C D Shao, Y Takashima, et al. Numerical investigation on fracture initiation properties of interface crack in dissimilar steel welded joints. *Chin. J. Mech. Eng.*, 2020, 33: 27.

[30] K Xu, X Wang, H Cui, et al. Investigation on LCF behavior of welded joint at different temperatures for bainite steel. *Chin. J. Mech. Eng.*, 2019, 32: 29.

[31] S L Li, Q Liu, S S Rui, et al. Fatigue crack initiation behaviors around defects induced by welding thermal cycle in superalloy IN617B. *Int. J. Fatigue*, 2022, 158: 106745.

[32] K J Li, X Wang, S S Rui, et al. Fatigue crack growth mechanism of Ni-based weld metal in a 9% Ni steel joint. *Mater. Sci. Eng. A*, 2022, 832: 142485.

[33] X G Li, B M Gong, X G Liu, et al. Effects of hydrogen and microstructure on tensile properties and failure mechanism of 304L K-TIG welded joint. *Mater. Sci. Eng. A*, 2018, 735: 208-217.

[34] J D Parker, G C Stratford. Characterization of microstructures in nickel based transition joints. *J. Mater. Sci.*, 2000, 35(16): 4099-4107.

[35] R D Nicholson. Creep-rupture properties of austenitic and nickel-based transition joints. *Met. Technol.*, 1982, 9: 305-311.

[36] M Yamazaki, T Watanabe, H Hongo, et al. Creep rupture properties of welded joints of heat resistant steels. *J. Power Energy Sys.*, 2008, 2(4): 1140–1149.

[37] J Akram, P R Kalvala, M Misra, et al. Creep behavior of dissimilar metal weld joints between P91 and AISI 304. *Mater. Sci. Eng. A*, 2017, 688: 396-406.

[38] R L Klueh, J F King. Austenitic stainless steel-ferritic steel weld joint failures. *Weld. J.*, 1982, 61(9): 302s–311s.

[39] X G Li, J F Nie, X Wang, et al. Evolution mechanism of interfacial microstructure and its effect on failure in dissimilar metal welds containing ferritic heat resistant steels. *J. Mater. Res. Technol.*, 2023, 26: 6565-6580.

[40] X G Li, Z P Cai, X Chen, et al. Characterization and formation mechanism of ultra-fine ferrite grains in dissimilar metal weld between austenitic stainless steel and low alloy ferritic steel. *Mater. Charact.*, 2021, 171: 110777.

[41] P Parameswaran, K Laha. Role of microstructure on creep rupture behaviour of similar and dissimilar joints of modified 9Cr-1Mo steel. *Procedia Eng.*, 2013, 55: 438-442.

[42] J N Dupont. Review of dissimilar metal welding for the NGNP helical-coil steam generator. In: E. United States (Ed.), Office of the Assistant Secretary for Nuclear, Idaho National Laboratory, 2010.

[43] Y Zhang, M Hu, Z P Cai, et al. Effect of nickel-based filler metal types on creep properties of dissimilar metal welds between Inconel 617B and 10% Cr martensitic steel. *J. Mater. Res. Technol.*, 2021, 14: 2289–2301.

[44] J N Hu, E Elmukashfi, T Fukahori, et al. Effect of weld angle on the creep rupture life of ferritic/austenitic dissimilar weld interfaces under remote mode I fracture. *Eng. Fract. Mech.*, 2019, 218: 106606.

[45] Y Wang, C Shao, S Huang, et al. Effect of CrN coating on interfacial creep crack initiation behavior for steel/Ni dissimilar metal welded joint. *Metall Mater Trans A*, 2022, 53: 3817-3822.

[46] J DuPont, S Babu, Z Feng. Development of novel functionally graded transition joints for improving the creep strength of dissimilar metal welds in nuclear applications. Lehigh Univ., Bethlehem, PA (United States), 2018.

[47] M Subramanian, J Galler, J DuPont, et al. Heterogeneous creep deformation behavior of functionally graded transition joints (GTJs). *Weld World*, 2021, 65: 1633-1644.

[48] K J Li, J Y Liu, Z P Cai, et al. Microstructure and creep properties of graded transition joints between nickel-based alloys and martensitic heat-resistant steels. *Mater. Sci. Eng. A*, 2023, 872: 144962.

[49] J H Yang, C K Song, Q T Wang. Comparative analysis of the effects of aggregates and fibres on the fracture performance of lightweight aggregate concrete based on types I and II fracture test methods. *Theor. Appl. Fract. Mec.*, 2022, 117: 103202.

[50] X G Li, Z P Cai, X Chen, et al. Oxidation damage and interfacial failure of dissimilar metal welds containing ferritic heat resistant steels. *J. Iron Steel Res. Int.*, 2021, 28: 1439-1450.

[51] J Zhang, Y Tang, G Zhang, et al. Numerical simulation on interfacial creep failure of dissimilar metal welded joint between HR3C and

T91 heatresistant steel. *J Wuhan Univ Technol -Mater Sci Ed*, 2016, 31(5):1068-1074.
[52] J F Wen, S T Tu, X L Gao, et al. New model for creep damage analysis and its application to creep crack growth simulations. *Mater. Sci. Tech-Lond*, 2014, 30(1): 32–37.
[53] M Tabuchi, H Hongo, Y Li, et al. Evaluation of microstructures and creep damages in the HAZ of P91 steel weldment. *J Pres Vessel Technol*, 2009, 131(2): 21406.
[54] M K Brun, R N Singh. Effect of thermal expansion mismatch and fiber coating on the fiber/matrix interfacial shear stress in ceramic matrix composites. *J. Am. Ceram. Soc.*, 1988, 3(5): 506-509.
[55] Y Gao, H M Yao. Homogenizing interfacial shear stress via thickness gradient. *J. Mech. Phys. Solids*, 2019, 131: 112-124.
[56] D Kobayashi, M Miyabe, Y Kagiya, et al. An assessment and estimation of the damage progression behavior of IN738LC under various applied stress conditions based on EBSD analysis. *Metall. Mater. Trans. A*, 2013, 44(7): 3123–3135.
[57] S S Rui, Y B Shang, Y N Fan, et al. EBSD analysis of creep deformation induced grain lattice distortion: A new method for creep damage evaluation of austenitic stainless steels. *Mater. Sci. Eng. A*, 2018, 733: 329-337.

Xiaogang Li born in 1992, is currently an assistant Professor at *Institute of Nuclear and New Energy Technology, Tsinghua University, China*. He received his PhD degree from *Tsinghua University, China*, in 2022.

Junfeng Nie born in 1982, is currently an associate Professor at *Institute of Nuclear and New Energy Technology, Tsinghua University, China*. He received his PhD degree from *Tsinghua University, China*, in 2009.

Xin Wang born in 1979, is currently a Research Engineer at *Institute of Nuclear and New Energy Technology, Tsinghua University, China*. He received his Master degree from *Tsinghua University, China*, in 2009.

Kejian Li born in 1989, is currently an associate Professor at *Department of Mechanical Engineering, Tsinghua University, China*. He received his PhD degree from *Tsinghua University, China*, in 2016.

Haiquan Zhang born in 1970, is currently a Professor at *Institute of Nuclear and New Energy Technology, Tsinghua University, China*. He received his PhD degree from *Beihang University, China*, in 2002.